

Fabrication of Graphene Oxide and Graphene Foams for Li-ion Batteries

By

Bahareh Bakhtiari

Submitted to the Graduate School of Engineering and Natural Sciences

In partial fulfillment of the requirements for the degree of

Master of Science

Sabanci University

Dec 2019

Fabrication of Graphene Oxide and Graphene Foams for Li-ion Batteries

APPROVED BY:

Prof. Dr. Selmiye Alkan Gürsel
(Thesis Supervisor)

Asst. Prof. Dr. Alp Yürüm
(Thesis Co-Supervisor)

Assoc. Prof. Dr. Emre Erdem

Asst. Prof. Dr. Mustafa Kemal Bayazıt

Asst. Prof. Dr. Burcu Dedeoğlu


.....


.....


.....


.....

DATE OF APPROVAL: 09.12.2019

TO MY MOM & SISTER

© By Bahareh Bakhtiari 2019
All Rights Reserved

ABSTRACT

Fabrication of Graphene Oxide and Graphene Foams for Li-ion Batteries

Bahareh Bakhtiari

Materials Science and Nano Engineering, M.Sc. Thesis, 2019

Thesis Supervisor: Prof. Dr. Selmiye Alkan Gürsel

Thesis Co-supervisor: Asst. Prof. Dr. Alp Yürüm

Keywords: Graphene, graphene oxide, graphene foam, graphene aerogel, CVD method

Graphene based materials are very promising owing to their fascinating characteristics such as extremely tunable surfaces, outstanding electrical conductance, good chemical stability and outstanding mechanical performance for energy storage applications. This project summarizes recent developments on 3D graphene network electrodes for Li-ion battery applications. A foam-like graphene material can be prepared by chemical vapor deposition and hydrothermal reduction of graphene oxide suspensions. The graphene foam has a much higher capacity than conventional graphite anode, and it possesses better rate capability as compared to powder like graphene active materials.

A new super-light graphene aerogel (GA) was effectively synthesized with a high electrical technique using a low cost and accessible method. More importantly, our synthesis approach compared to the common graphene oxide (GO) reduction temperature (180 °C) involves low temperature (95°C) where the promising GO reduced with different reducing agents is achieved through freezing. In this work, we systematically investigate the effects of various reducing agents including ammonia, hydro-iodic acid, and ascorbic acid at different hydrothermal reaction time (4, 8, 24 hours) and reducing agent dosages (0, 50, 120, 200 μL) on the formation of foam, electrical conductivity, and morphology of GA. The results reveal that graphene aerogel reduced by ascorbic acid possesses the most outstanding performance on mechanical strength and reutilization but has moderate electrical conductivity (9.4 S/m). Whereas, the sample obtained with HI exhibits the highest electrical conductivity (12.1 S/m). However, this sample reveals poor mechanical strength. The graphene aerogel reduced by ammonia is very sensitive to the reaction time and temperature and has moderate mechanical strength and the lowest electrical conductivity (7.5 S/m). Therefore, ascorbic acid is a very promising reducing agent for the hydrothermal process as the resulted graphene aerogel had good electrical conductivity and great mechanical strength.

ÖZET

Li-iyon Bataryalar İçin Grafen Oksit ve Grafen Köpüklerin Üretimi

Bahareh Bakhtiari

Malzeme Bilimi ve Mühendisliği, MSc Tezi, 2019

Tez Danışmanı: Prof. Dr. Selmiye Alkan Gürsel

Ortak Tez Danışmanı: Yrd. Doç. Dr. Alp Yürüm

Anahtar Kelimeler: Grafen, Grafen Oksit, Grafen köpük, Grafen aerojel, CVD metot

Günümüzde grafen destekli malzemeler, ayarlanabilir yüzeylere sahip olmaları, kimyasal stabilizeleri, mekanik dirençlere dayanıklı olma gibi özelliklerinden dolayı umut vadeden malzemeler olarak bilinmektedir. Bu gibi özelliklerinin yanında grafen destekli malzemelerin üretim tekniklerinin geniş ve düşük maliyetli olması bu malzemelerinin kullanım alanlarının genişletilmesinde etkilidir.

Bu yüksek lisans projesinde grafenin lityum iyon bataryalarına olan katkısı amaçlanmaktadır. Projede kimyasal buhar yöntemi kullanılarak biriktirilen grafen oksit süspansiyonlarının hidrotermal reaksiyonlar ile indirgenmesiyle elde edilen çoklu bir sentez metotluyla üretilen grafen ve grafen oksit detaylı bir şekilde anlatılmıştır. Bu metot ile üretilen grafen çok

türevlerine göre çok daha yüksek bir kapasiteye sahiptir. Bu özelliğinin yanında türevlerine göre daha hafiftir. Daha da önemlisi bu teknik ile sentezlenen grafen oksitler diğer yöntemlere göre üretilen grafen oksitlere; indirgenme sıcaklığı (95°C) yönünden kıyaslandığında çok daha düşük bir sıcaklık ile indirgenmenin tamamlandığı gözlenmiş olup, farklı hidrasyon süreleriyle (4, 8, ve 24 sa.) birlikte farklı miktardaki indirgenme reaksiyonlarındaki ajanların (0, 50, 120 ve 200 µL) etkilerinin malzemeye olan etkileri de incelenmiştir.

Öte yandan elde edilen sonuçlarda askorbik asit ile indirgenmiş olan malzemenin mekanik mukavemet ve yeniden kullanımda en üstün performansa sahip olduğunu ancak orta derecede elektriksel iletkenliğe (9.4 S/m) sahip olduğunu, oysa HI ile elde edilen numune en yüksek elektriksel iletkenliğine (12.1 S/m) sahip olduğunu ve askorbik asitin malzeme için en iyi elektriksel iletkenliğe sahip olmasındaki önemini açıklamıştır.

ACKNOWLEDGMENT

I would first like to thank my thesis supervisor, Prof. Selmiye Alkan Gürsel, for her useful remarks, comments and engagement through the learning process of this master thesis, and also for her continuous support. Her patience, motivation, enthusiasm, and immense knowledge and her guidance has helped me during this period.

I would also like to thank Dr. Alp Yürüm and Dr. Sibel Kasap for their involvement in this research project. Without their intense participation and input, the survey could not have been successfully managed. I am also thankful to the members of our group for their forbearance and support in helping me overcome obstacles during my research.

Besides my advisor, I would like to thank the rest of my thesis jury: Dr. Burcu Dedeoglu, Dr. Emre Erdem, and Dr. Mustafa Kemal Bayazıt for their encouragement and insightful comments. I would like to thank my fellow lab mates in SUNUM: Adnan Taşdemir, Shayan Mehraeen, Buse Bulut Köpüklü and Pozhhan Mokhtari for discussions and all the fun we have had in the last two years.

Last but not the least, I would like to thank my family especially my mom for supporting me throughout my life and my sister (Rokhsareh) for supporting me throughout this thesis writing and my life in general.

TABLE OF CONTENT

ABSTRACT.....	v
ÖZET	vii
ACKNOWLEDGMENT.....	ix
TABLE OF CONTENT	x
LIST OF FIGURES	xii
LIST OF TABLES.....	xiv
CHAPTER 1	1
INTRODUCTION	1
1.1 Lithium-Ion Batteries –Materials Development and Status.....	1
1.1.1 Anode Materials.....	2
1.1.1.1 Conversion Anodes.....	4
1.1.1.2 Intercalation Materials in Batteries	5
1.1.1.3 Foam Structured Electrode.....	5
1.2 Introduction to Graphene, and Graphene Oxide Properties and Applications.....	7
1.3 Reducing Agents.....	10
1.3.1 Ascorbic Acid	11
1.3.2 HI	13
1.3.3 NH ₃	15
1.4 Preparation Methods of 3D Graphene Networks	16
1.4.1 Chemical Vapor Deposition (CVD) Growth Methods.....	17
1.4.2 Direct Self-Assembly Of Graphene Oxide.....	18
1.4.3 Hydrothermal Reduction Induced Self Assembly.....	19
CHAPTER 2	21
MATERIALS & METHODS	21
2.1 Materials.....	21
2.1.1 Graphene Oxide Synthesis with Chemical Exfoliation Technique.....	21
2.2 Fabrication of Graphene Networks	23
2.2.1 Template-Assisted Chemical Vapor Deposition Growth (CVD).....	23

2.2.2 Graphene Aerogel (GA) Synthesis.....	24
2.3 Self-Assembled Fe ₂ O ₃ /Graphene Aerogel	26
2.3.1 Preparation of Fe ₂ O ₃ -Graphene Composites	26
2.4 Electrochemical Characterization Studies.....	26
CHAPTER 3	27
RESULTS & DISSCUSSION	27
3.1 Structural and Electrochemical Properties of Graphene Aerogel (Part 1)	27
3.1.1 Thermal Characterization.....	27
3.1.2 XRD and Raman Characterization.....	28
3.1.3 SEM Characterization	32
3.1.4 Electrical Conductivity Analysis.....	34
3.1.5 Mechanical Characterization.....	36
3.1.6 Effect of Different Reducing Agent on Graphene Aerogel Properties	36
3.1.7 Effect of synthesis time on Graphene Aerogel Properties	37
3.1.8 Effect of Reducing Agent Dosage on Graphene Aerogel Properties	38
3.2 Structural and Electrochemical Properties of Graphene Foam Prepared with CVD Method (Part 2).....	39
3.2.1 XRD and Raman Characterization.....	39
3.2.2 SEM Characterization CVD.....	40
3.2.3 Electrochemical Characterization	41
CHAPTER 4	44
CONCLUSION	44
4.1 Conclusion	44
5. REFERENCES.....	46

LIST OF FIGURES

Figure 1. 1 (a) the charge transport pathways in a conventional electrode with a 2D current collector show a limited charge penetration depth. (b) The charge transport pathways in a 3D thick electrode show efficient charge delivery throughout the entire electrode thickness [27]	6
Figure 1. 2 The graphene structure: Monolayer structure of all-sp ² carbon atoms arranged in 2D lattice.....	9
Figure 1. 3 Graphene (a) foam, (b) aerogel	10
Figure 1. 4 The molecules of ascorbic acid and dehydroascorbic acid [34].....	11
Figure 1. 5 The reduction mechanisms of ascorbic acid suggested by Gao et al [46].....	12
Figure 1. 6 Synthesis procedure of template-directed CVD approach for GFs.....	18
Figure 1. 7 (a) Graphene, (b) graphene oxides containing one epoxy functional group, (c) Charge transfer dependence on the applied electric field in +E along graphene, (d) the net electron-charge transfer from NH ₃ to graphene	16
Figure 1. 8 Synthesis procedure of template-directed CVD approach for GFs	18
Figure 2. 1 (a) GO synthesis setup, (b) GO suspension before washing, (c) GO suspension after precipitation, (d) Washing process with special centrifuge tube, (e) Collection of the sample, (f) Dried final GO product.....	22
Figure 2. 2 (a) Ni foam, (b) Ni-Graphene foam before etching in FeCl ₃ /HCL solution, (c) Graphene foam after etching in DI water, (d) Drying Ni foam in 55 C, (e) Graphene foam	24
Figure 2. 3 Synthesis of graphene aerogels: (a) GO aqueous dispersion, (b) graphene hydrogel, (c) washed graphene aerogels and (d) dried graphene aerogels.	25
Figure 3. 1 Thermogravimetric analysis of 3D graphene foam/ Fe ₂ O ₃ prepared with hydrothermal reduction method.....	28
Figure 3. 2 Raman spectra of GO and GAs reduced by ammonia, ascorbic acid, and HI at 95°C.....	29
Figure 3. 3 Raman spectra of GA and Fe ₂ O ₃ /GA prepared with ascorbic as a reducing agent in 95 °C.....	30

Figure 3. 4 XRD patterns of GA and Fe ₂ O ₃ /GA prepared with ascorbic as a reducing agent in 95 °C.....	31
Figure 3. 5 SEM images of the GAs prepared by (a) ammonia, (b) ascorbic acid at 95°C..	32
Figure 3. 6 SEM images of graphene aerogel prepared using GO dispersions at different concentration of (a) 4 (b) 5, (c) 10 (d) 30 mg mL ⁻¹	33
Figure 3. 7 Typical SEM images of Fe ₂ O ₃ /GAs revealing the 3D microporous structure and uniform distribution of Fe ₂ O ₃ particles.....	34
Figure 3. 8 GAs ' electrical conductivity with different reducing agents.	35
Figure 3. 9 Optical images showing high compressibility of graphene aerogel.....	36
Figure 3. 10 Appearance of the prepared graphene hydrogel after the GO (4 mg mL ⁻¹) reacted with ammonia solution at 95°C for different reaction times	37
Figure 3. 11 Appearance of the prepared graphene hydrogel after the GO (4 mg mL ⁻¹) reacted with different dosage of ammonia at 95 °C.....	38
Figure 3. 12 XRD patterns of graphene foam and pure nickel foam.....	39
Figure 3. 13 Raman spectra of graphene foam prepared with CVD method in 10 and 20 minutes.....	40
Figure 3. 14 SEM images of (a) bare 3D Ni foam, (b) Nickel-Graphene foam (graphene deposited on the Ni foam), and (c) Graphene foam.....	41
Figure 3. 15 Cyclic voltammetry of graphene foam at a scan rate of 0.1 mV.S ⁻¹	42
Figure 3. 16 Discharge/Charge profiles of graphene foam at current rate of 0.4 mA.Cm ⁻² between 0.01 and 3 V: the discharge curves in the first, 20 th , 50 th , 100 th	43
Figure 3. 17 Cycling performance of graphene foam at the current density of 185 mA.g ⁻¹	43

LIST OF TABLES

Table 1. 1 Different Types of Anode Materials [21]	4
Table 1. 2 Chemical properties of graphene family nanomaterials [30].	8

CHAPTER 1

INTRODUCTION

1.1 Lithium-Ion Batteries –Materials Development and Status

A lithium-ion battery includes a cathode (such as, metal oxide) and an anode (graphite) which are separated by a conducting electrolyte, LiPF₆-ethylene carbonate-diethyl carbonate, for instance. The chemical and physical properties of the positive and negative electrodes have a huge effect on the performance and energy density of lithium-ion battery. Some parameters play a vital role in improving the cathode materials, for example, high potential and structural stability. There is still a high capacity for new anode with reversible lithium storage capacity [1]. There should be some increase in the energy densities (Wh/kg) for developments in the mobile device sector and in other applications related to aerospace, automotive, and flexible electronic devices [2].

In recent years, graphene as an anode material has been researched significantly due to its 2D structure which leads to higher capacity when compared to graphite [3]. Replacing the carbon anode with new material is an alternative path to increase the energy density of lithium-ion batteries. The theoretical capacity of the graphite is 372 mAh/g, which is only about one-tenth of Li [4-7]. Due to the formation of the lithium anode surface, the use of lithium metal in the electrolyte solution is a problem which researchers are seeking a solution for. Nowadays, new high-capacity anode materials such as alloys, metal oxides with carbon-based composites are being examined [8, 9].

To increase the power density and energy for future targets of energy storage, sort of attempts have been done to promote nano active materials for lithium-ion batteries. The advantages of the nano active materials and their solutions were investigated. On the other hand, disadvantages of these materials were evaluated. The main drawbacks of nano active materials, that limit the total volumetric energy density of lithium-ion batteries is the low packing density.

1.1.1 Anode Materials

There are some parameters which affect the anode material based on its characteristics such as, quick and high insertion kinetics, and redox versus Li capacity. It is very important for the anode material to keep its structural abilities without any loss of electrical contact even after repeated charging cycles. As the lithium intercalation compounds are generally made by graphite, most of the anode's changes introduced over the past century include carbonaceous materials [6-10, 12]. The reason behind the business achievement of carbon-based adverse electrodes includes the comparatively small intrinsic carbon price, its outstanding lithium insertion reversibility, and the formation of positive surface film with many electrolyte alternatives. Recently, carbon and lithium alloy metals are the most prevalent among anode materials. The host element in the compound/alloy of graphite intercalation "shields" the lithium inserted, making the alloy less sensitive to electrolytes. As a result, in the lithiated material, the chemical potential of lithium is lower than in metallic

lithium. This translates into a safety benefit, but with a penalty in cell voltage and hence also in energy and power density [13-17].

In addition, the load-discharge efficiency of these alternative anode components also relies on the lithium diffusion rate in the matrix of the host [18]. Lithium-storing metals are among the most attractive and competitive applicants in lithium-ion batteries for fresh kinds of anodes (adverse electrodes). Indeed, several metals and semiconductors, such as aluminum, tin and silicon, respond with lithium to form alloys through partly reversible and low voltage (relative to lithium) electrochemical procedures, require many atoms per formula unit, and provide a much bigger specific capacity than standard graphite [13, 19].

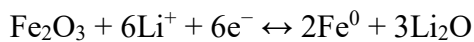
Unfortunately, accommodating so much lithium in the host metal plus phase transitions are followed by huge volume modifications. During the alloying/de-alloying procedures, the mechanical strain produced leads to the cracking and crumbling of the metal electrode and a marked loss of storage ability over a few cycles. While these structural modifications are prevalent in alloying responses, efforts have been made to restrict their side effects on the integrity of the electrode [14-16]. One appealing path is the active/inactive nano-composite idea [20]. This includes mixing two materials closely, one responding with lithium was, like the other, acting as an inactive confining buffer. Within this composite, the use of metallic nano-sized clusters as lithium hosts significantly suppresses the related strains and thus improves the alloying response reversibility. Table 1.1 lists the various anode material kinds.

Table 1. 1 Different Types of Anode Materials [21]

Material	Theoretical Capacity (mAh/g)	Practical Capacity (mAh/g)	Problems
Graphite	372	250	Low charge capacities
Silicon	4200	2158	Large volume expansion and high capacity fade per cycle
Tin	994	400	Large volume expansion and high capacity fade per cycle
Metal Oxide Composites (Co, Mn, Fe)	880	700	Large volume expansion
Graphene	744	350	Large voltage hysteresis between charge discharge profiles
Graphene Alloy Composites (Si)	2500	1168	

1.1.1.1 Conversion Anodes

The recent interest onto the new reactivity concept with electrochemical reaction of lithium which is reversible with metal oxides transitions can be referred as “conversion reaction” is as follow:



In this reaction, M is a transition metal (Sc, Ti, V, Cr, Mn, Fe, Co, Ni, Cu, Zn), and X is going to be O, P, F, N and S [22]. In converted materials, the perfect reduction of M_aX_b to metallic nanoparticles, which has large surface, are active in Li_nX matrix decomposition and keeps them together. The size of these particles in term of nanometric scale seems to be maintain after several cycles [22-24].

Unfortunately, these materials present several issues. The most relevant are [25]:

- The structural reorganization induces, as for the alloy-based materials, big volume changes, resulting in particles de-cohesion and subsequent cell failure.
- Unacceptable large voltage hysteresis between discharge and charge steps.
- Large Coulombic inefficiency observed in the first cycle.
- Low conductivity.

The reduction/conversion (lithium uptake) reaction will always occur on battery discharge, while the reverse will occur during charge (lithium release).

Hence, despite the progress made with these materials, several issues persist in the way to making them a viable alternative [25, 26].

1.1.1.2 Intercalation Materials in Batteries

Intercalation can be identified as to insert among the layers in crystal lattice, geological formation, or other structure. Generally, the “intercalation” refers to the reversible inclusion or molecule insertion into layered structure compounds. During the charging and discharging process the Li-ion batteries intercalation is happening, such as the other batteries that include positive and negative electrode and electrolytes. During the discharge process, the positive lithium starts from the negative electrode (e.g. graphite) and enters the positive electrode (e.g. lithium oxide) through the electron solution that is usually prepared with organic solvent in solid or liquid form). While charging, the reverse process is happening and that is why, it is called as reversible process.

1.1.1.3 Foam Structured Electrode

As a consequence of the charge transport limit, a typical 2D electrode with a planar current collector can provide sufficient charge to satisfy the charge requirement of the electrode material but at a limited depth. (Fig. 1.1a)

For a thicker electrode with high mass loading beyond such depth limits, only a portion of the active material is actively used for energy (charge) storage because of insufficient charge delivery. By contrast, a 3D electrode architecture contains a 3D conductive scaffold acting as a 3D current collector and a 3D porous network for efficient ion transport. This structure ensures efficient charge delivery throughout the bulk volume of a thick electrode (Fig. 1.1b), which is desirable for the utilization of all electrode materials regardless of the electrode thickness and for the realization of high-rate and high-capacity energy storage. In this regard, 3D carbon frameworks are attractive scaffolds for the efficient loading of active materials because of their high surface area, low density, excellent conductivity and superior electrochemical stability compared with other conductive materials.

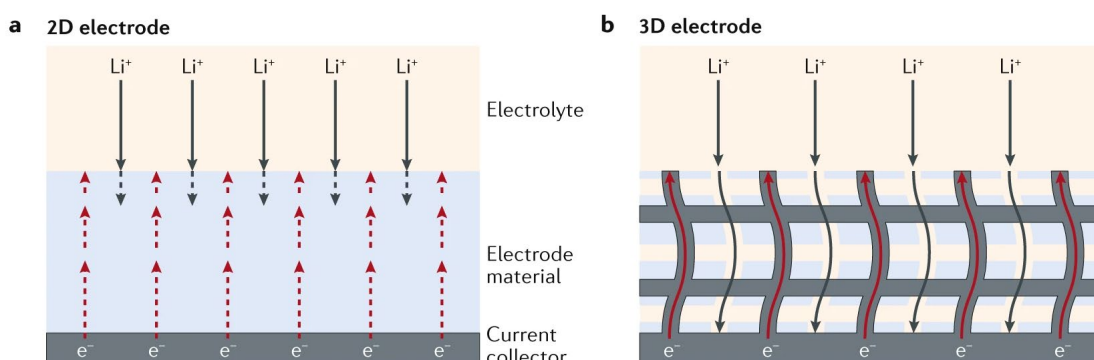


Figure 1. 1 (a) the charge transport pathways in a conventional electrode with a 2D current collector show a limited charge penetration depth. (b) The charge transport pathways in a 3D thick electrode show efficient charge delivery throughout the entire electrode thickness

[27]

1.2 Introduction to Graphene, and Graphene Oxide Properties and Applications

Graphene is a well-known two-dimensional natural material with monolayer structure of all- sp^2 carbon atoms with some of the most fascinating properties such as lightweight, high thermal, mechanical, electrical properties along with a very large active surface area.

At desirable conditions, graphene with high mechanical strength (tensile strength of 130 GPa - Young's modulus of 1 TPa), excellent thermal conductivity ($5000 \text{ Wm}^{-1}\text{K}^{-1}$), and strong chemical durability and high electron mobility ($20 \text{ m}^2\text{V}^{-1}\text{s}^{-1}$) can be obtained [28]. These properties empower graphene and graphene-based materials to find applications in high-performance structural nanocomposites, electronics, and environmental and energy devices including both energy generation and storage [29]. Table 1.2 illustrates the difference between single layer graphene, graphene oxide and reduced GO.

Table 1. 2 Chemical properties of graphene family nanomaterials [30].

Property	Single layer graphene	Graphene oxide (GO)	Reduced GO
Young's modulus	1000 GPa	220 GPa	Not available
Fracture strength	130 GPa	120 MPa	Not available
Optical transmittance	97.7%	N/A (expected to be lower due to functional groups and defects)	60–90% depending on the reduction agent and fabrication method
Charge carrier concentration	$1.4 \times 10^{13} \text{ cm}^{-2}$	N/A (much lower due to more organic nature, functional groups and defects)	Not available
Room temperature mobility	$\sim 200,000 \text{ cm}^2 \text{ V}^{-1} \text{ s}^{-1}$	N/A (expected Much lower than 15,000 due to interruption in mobility by defects scattering)	expected to be intermediated of two due to less defects
Thermal conductivity	$\sim 5000 \text{ W/mK}$	2000 W/mK for pure 600 W/mK on Si/SiO ₂ substrate	0.14–0.87 W/mK
Electrical conductivity	10^4 S/cm	10^{-1} S/cm	200–35,000 S/cm

The precious graphene properties can be preserved in composite or bulk material [25]. It is possible to observe the reduction of high conductivity and mechanical strength of graphene sheets due to the agglomeration. The porous structure of graphene foam and the significant graphene properties, the result of the 3D structure is the powerful mechanical strength, high specific surface area and electron transport kinetics [26]. Various methods were used to prepare 3D networks of graphene. 3D structure of graphene can be used in sensors, energy storage, conversion and catalyst [27]. The common way to provide the 3D structure is by linking the individual sheets to form three-dimensional (3D) networks. So, it is prevented to single graphene sheets form repositioning [28-30]. Figure 1.2 shows the graphene structure.

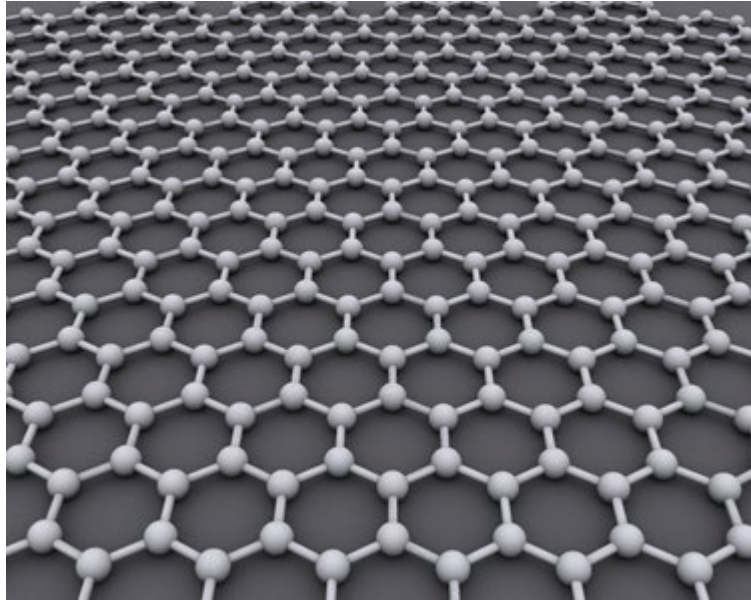


Figure 1. 2 The graphene structure: Monolayer structure of all-sp² carbon atoms arranged in 2D lattice.

Significant attempts have also been made to create 3D graphene networks (3DGNs) synthesis and applications with different morphologies, structures, and characteristics. The common 3D graphene networks were investigated in different studies are graphene foams (GFs), graphene sponges (GSs) and graphene aerogels (GA) [31].

GFs (see Fig.1.3a) were synthesized as the template for the first time by using nickel foam. Thus, with a constant and interconnected 3DGN, the GFs acquired the nickel foam's Micron-sized structure. GSs have a comparable porous structure to GFs, but the graphene sheets are almost aligned to each other or partly oriented, producing an anisotropic lamellar structure [32-33]. GSs are named like sponges because of their highly efficient and recyclable absorption performance [34].

GAs (see Fig.1.3b) are generally manufactured using sol gel chemistry that includes lowering graphene oxide to create a highly cross-linked graphene hydrogel, followed by freeze-drying or supercritical drying to remove the water absorbed. Although their structures and characteristics differ, GFs, GSs and GAs all have outstanding characteristics, such as high

electrical conductivity, high surface area, low density, high porosity, and good mechanical characteristics [35].

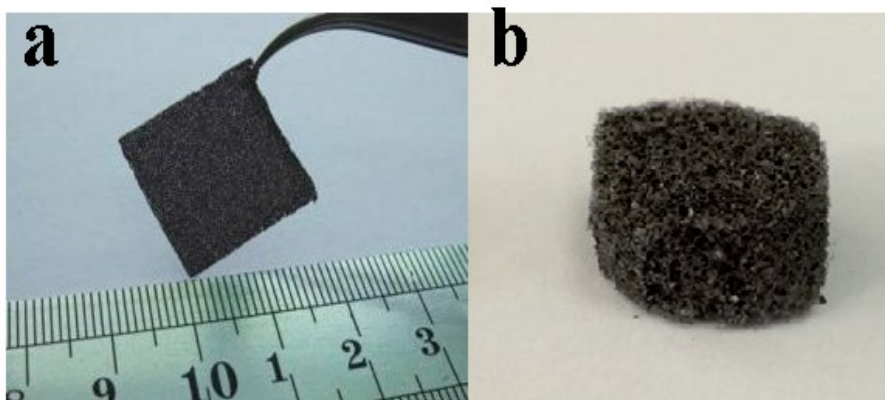


Figure 1. 3 Graphene (a) foam, (b) aerogel

1.3 Reducing Agents

Chemical reduction of GO is usually occurred in standard room temperature or by applying moderate heating and can be accomplished through chemical reagent reduction, photo catalyst reduction, electrochemical reduction, and solvo-thermal reduction methods. Chemical reduction of GO is more affordable and accessible for mass production of rGO compared to other methods like thermal reduction. Reducing agent in the form of gas and liquid is the main component of this method and by adding this agent to the GO, some functional groups can be eliminated. The known reducing agents are Phenyl hydrazine, hydroxylamine, hydroquinone, glucose, sodium borohydride, alkaline solution and pyrrole. In this study, it is attempted to control the other three agents' effect and their applicability. Ascorbic Acid, HI and NH_3 are the used reducing agents that are evaluated in this study.

1.3.1 Ascorbic Acid

One of the known reducing agents, is Ascorbic Acid which is also calls as C vitamin. This material is nontoxic, natural antioxidant that is using for GO reduction.

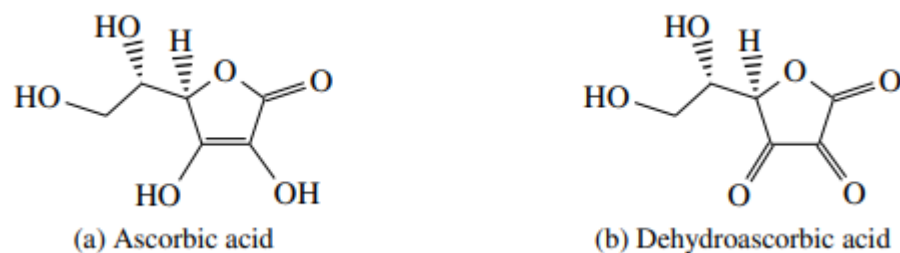
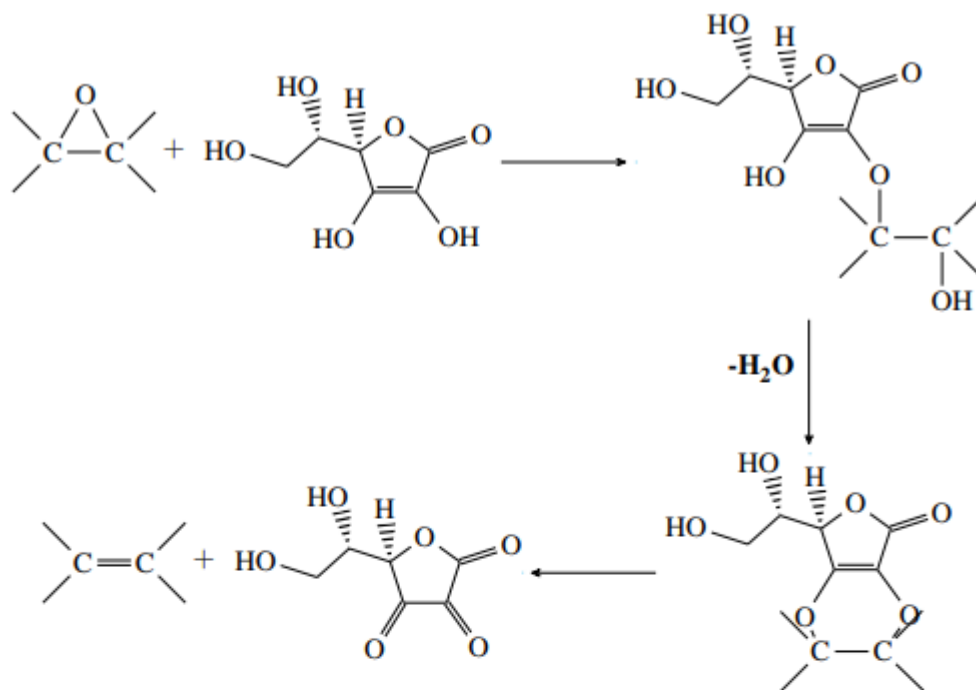


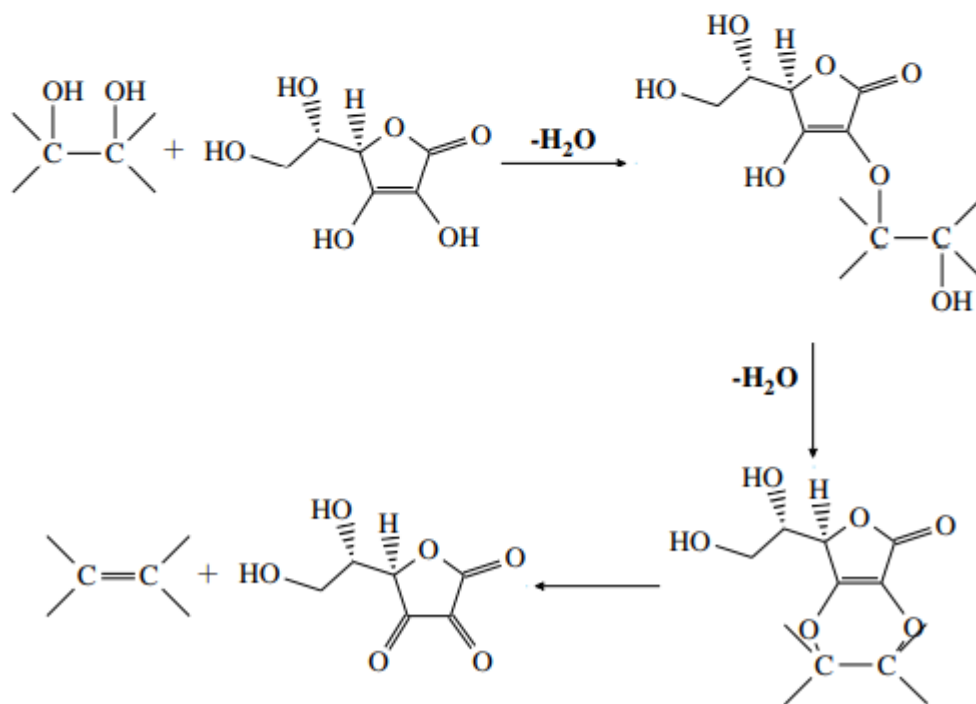
Figure 1. 4 The molecules of ascorbic acid and dehydroascorbic acid [34]

Fernandez-Merino et al [35] represents that AA can reduce GO as well as affecting on electrical conductivity of the same time as GO reduced by hydrazine. This findings reveals that it is not necessary to have a lower redox potential than AA to reduce GO. AA includes the standard redox potential $E^\circ = -0.39 \text{ V}$ [37] that is roughly one fourth for that of hydrazine with $E^\circ = -1.49 \text{ V}$ [38].

De Silva et al. [36] found out about two different regions of reduction of GO using AA. They are chased the GO reduction by utilizing UV-Vis and XPS. By employing these methods, they found that the primary regime of reduction lead to a reduction in CO-bonds and that the second regime reduces the amount of CO-Bonds. This findings confirm the results reported by Guex et al [40]. By reduction of GO which provide rGO the remained molecules ate not AA but dehydroascorbic acid (DHA) which is shown in figure 1.4b. Besides, the proposed reduction paradigm of hydroxyl and epoxide group present in GO using AA is illustrated in figure 1.5. AA greatly absorbs ultraviolet-light, evident from figure 1.6, but does not absorb visible light cause's transparent liquid.



(a) The reduction of an epoxide group



(b) The reduction of two OH groups

Figure 1. 5 The reduction mechanisms of ascorbic acid suggested by Gao et al [46]

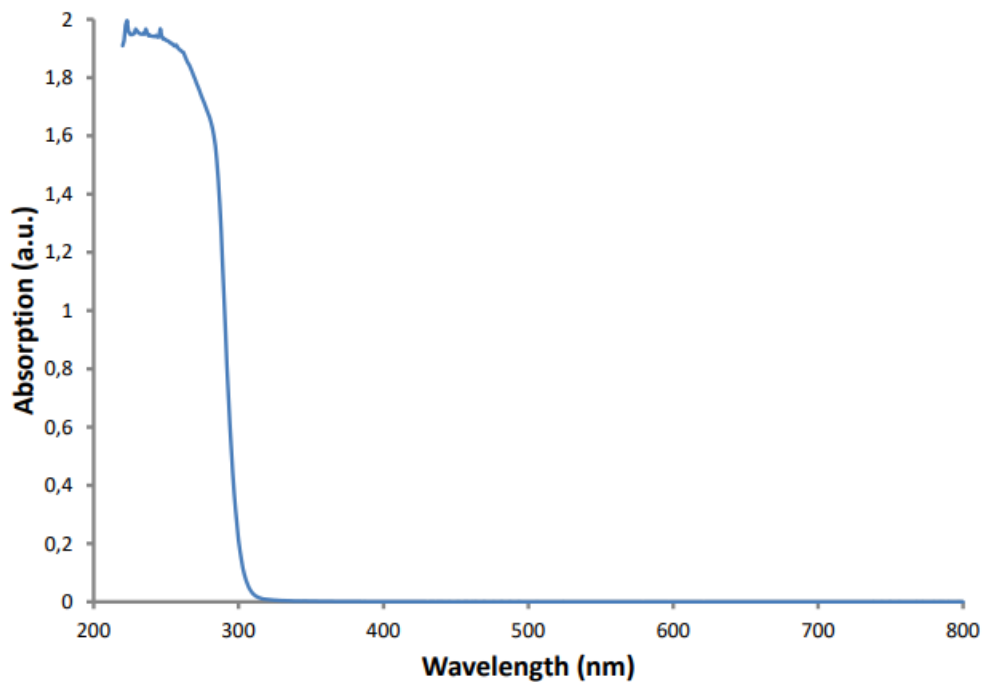


Figure 1. 6 UV-Vis absorption spectra of ascorbic acid [41]

1.3.2 HI

Hydroiodic acid (HI) is acidic solution of hydrogen iodide. It is one of the strong acid in hydrohalic acid group commonly use as chemical reagent. Several studies believe that HI has a reducing ability much higher than other reducing agents, in term of conductivity and mechanical properties. Hence, it is the proper reducing agent for GO to provide rGO [37]. The usual method is to immerse the GO sheet directly into hydroiodic acid (HI) solution in a sealed cuvette at room temperature for 1 hour. Then by washing the rGO-Hi sheet with DI water for several times and dried is room temperature, the final sheet electrode will be obtained. The average resistivity for GO samples which reduced by HI is to be in the range of 0.003 to 0.022 Ω .cm [44]. The XPS analysis results for GO sheets before and after reduction for evaluation of oxygen-containing groups' removal by HI acid can be interpreted. The C1s XPS spectrum of the as-prepared GO sheets significantly illustrate oxygen content with two components that correspond to carbon atoms in different functional groups. The CO bond carbon bonds (hydroxyl and epoxy, 286.4 eV), and the carbonyl carbon (CAO, 288.5

eV), in addition to the non-oxygenated ring carbon (CC, 284.6 eV), and carbon to oxygen (C/O) ratio (12) is more than any other reduction method. It seems that almost all of the oxygen-containing groups will be reduced during the HI reduction. This idea will give this hypothesis that for synthesis of large-area rGO sheets with good electrical conductivity is possible. This may ease the way for electrical property associated applications of large-area GO sheets.

The increment in interlayer spacing of graphite oxide is caused by oxygen-containing groups on the surface of graphene layers. This will also decrease the van der Waals interlayer interactions and makes easier cleave of layered graphite oxide. Simultaneously, on carbon atoms the oxygen-containing groups binding would change the graphene layer from planar sp^2 -hybridized to a distorted sp^3 -hybridized geometry [34-37]. It is investigated that the oxygen atom in triangular epoxy groups (COC) perform as minuscule wedge, pushing apart the bridge carbon atom and stretching the CC bond [35-38]. Consequently, the oxygen-containing formation significantly decrease the bond energy among carbon atoms through the carbon network. Wu et al., figured out the graphene sheets which derived chemically can be sono-chemically cut along parallel line faults on their surface to effectively fabricate graphene nanoribbons [37]. These nanoribbons will reveal the weaker interactions of stretched CC bonds or COC bonds than the normal CC bond [54]. By using the ultrasonic treatment, it is possible to separate the de-coupled graphene layers in graphite oxide. This will cause the formation of individual GO sheets. At the same time, the sono-chemical effects and ultra-hot gas bubbles could break the stretched CC bonds or COC bonds, leading to the cracking of graphene layers. Therefore, it is feasible to assume that the higher CO content in graphite oxide cause the layer cracking much easier. This is due to the more stretched CC bonds or COC bonds. The GO sheet with high CO content clearly shows the cracking of whole GO sheets after mild sonication while the low CO content behave vice versa. According to these findings, it could be assumed that the CO group's content of graphite oxide, can have a drastic role on controlling the area of the obtained GO sheets. This also provide applicable data about the area-controlled synthesis of GO sheets by chemical exfoliation.

1.3.3 NH₃

Ammonia is basically the compound of nitrogen and hydrogen which can be shown by NH₃ as chemical formula. It is also an active reducing agent because of presence of nitrogen atoms that include the “-3” oxidation number. Restorative properties of nitrogen are shown in term of ammonia combustion on air. The most stable nitrogen oxidation number is 0, the results is the free nitrogen. The ammonia and graphene oxide (GO) interaction is investigated by density functional theory calculations. The findings illustrate that the adsorption of ammonia and GO is usually more powerful than that on graphene. This is due to the existence of diverse active defect sites, such as the hydroxyl and epoxy functional groups and their neighboring carbon atoms. These surface oxygen sites can form OH...N and O...HN hydrogen bonds with ammonia and enhance charge transfers from ammonia to the graphene oxide. The absorbed ammonia is dissociating into a chemisorbed NH₂ or NH species through the H atom abstractions leads to hydroxyl group hydrogenation and ring-opening of epoxy group. It is believed that the reaction of ammonia, epoxy and hydroxyl is going to be exothermic with various energy barriers. This is depending on the atomic arrangement and oxidation species of these groups. Generally, the hydroxyl group exhibits shows the higher reactivity through hydrogen abstraction from the adsorbed ammonia comparing to the epoxy group in GO with single oxygen group. The OH group as neighborhood could activate the oxygen group to form the surface reaction on ammonia [38]. Pursuing the ring-opening of the epoxy group, the second H atom abstraction of NH₂ can remove the formed hydroxyl group. The evaluated state density of the adsorbed systems also represents strong interaction among ammonia and GO. The calculated results shows proper adjustment with experimental observation.

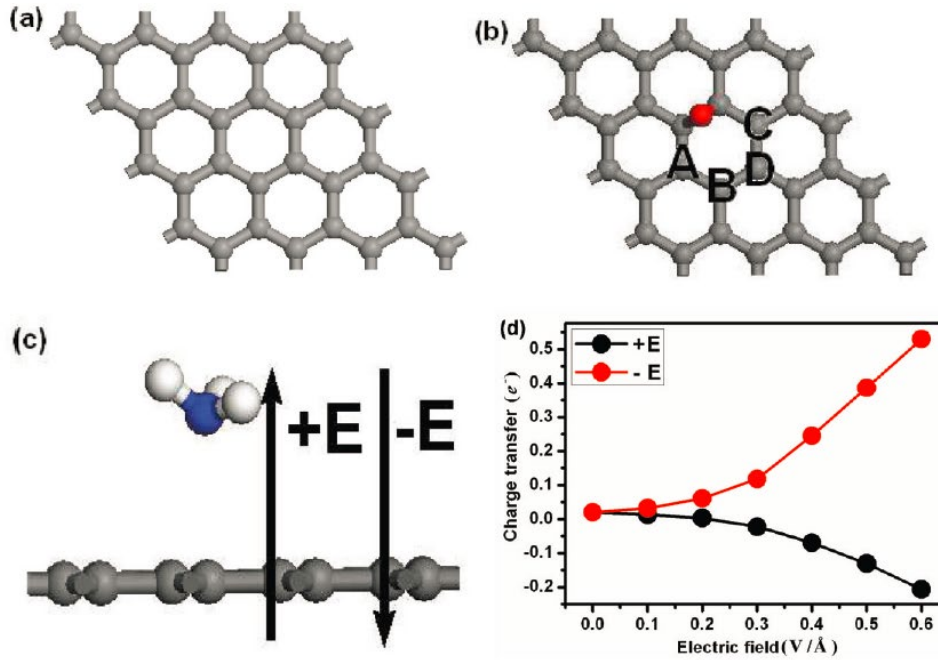


Figure 1.7 (a) Graphene, (b) graphene oxides containing one epoxy functional group. (c) Charge transfer dependence on the applied electric field in +E along graphene. (d) The net electron-charge transfers from NH₃ to graphene

1.4 Preparation Methods of 3D Graphene Networks

3D graphene materials have been mostly synthesized in various forms, namely graphene fibers, graphene tubes, graphene foams, graphene networks, and graphene sponges, graphene aerogels, and graphene with other 3D architectures. In order to obtain all of these structures, different methods of synthetic processing were used, which can usually be classified as direct synthesis of 3D-Graphene (chemical vapor deposition growth methods), self-assembly methods (hydrothermal-Reduction-Induced Self-Assembly, Direct Self-Assembly of Graphene Oxide) and other methods. In this project, two techniques are done: CVD method and the Self-assembly of GO through hydrothermal reduction [36].

Recently, the self-assembly of GO through hydrothermal reduction has attracted considerable attention due to low cost, high efficiency and non-pollution [37]. At the same time, three-dimensional (3D) graphene foam provides a possibility to solve the problem of low energy

density, which not only inherits the excellent properties of two-dimensional (2D) graphene, but also possesses some advantages involving light weight and higher porosity [38]. Therefore, the preparation and application of 3D graphene foam have become a hot research topic for both lab research and industrial production.

1.4.1 Chemical Vapor Deposition (CVD) Growth Methods

Chemical Vapor Deposition is one of the ways to grow 3D graphene which includes, using 3D metal substrates such as Ni or Cu foam that it is acting as both a catalyst and a template here. Porous nickel or Cu foam was exposed at 800-1000 ° C to carbon sources gases or liquids like methane gas, and at a steady pressure. In our work, at high temperatures on the surface of the Ni, carbon atoms are produced via the process of methane deposition [39-40]. Methane decomposition is described by the chemical reaction as following:



To remove the nickel, HCl or FeCl₃ solutions is used to produce freestanding graphene.

The CVD method can be divided into three categories: 1) atmospheric pressure CVD, 2) low-pressure CVD and 3) ultra-high vacuum CVD, according to its operating pressure.

One of the features of the typical CVD experiment is that the substrate is in the middle of a vacuum chamber or tube furnace. To make it possible to enable the reaction of volatile precursors to react on the surface of the substrate, it is important for the presence of additional catalysts and high-temperature treatment. According to Figure 4, in the case of sensitive materials to oxygen, a high vacuum environment and inert gases like Argon are applied for the protection of the products from oxidation.

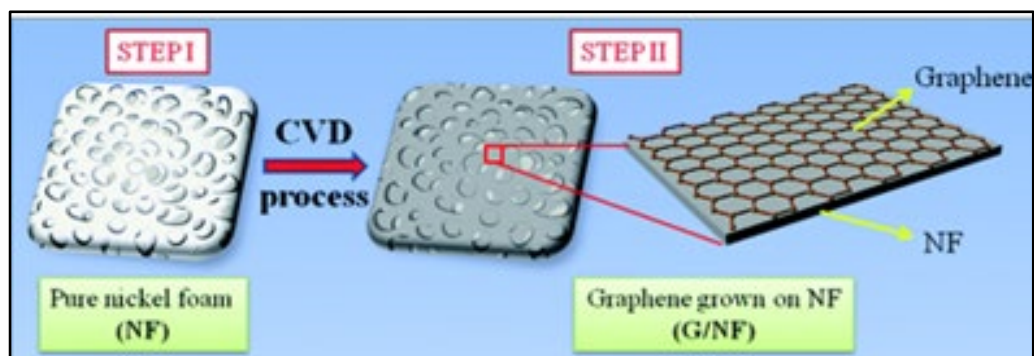


Figure 1. 8 Synthesis procedure of template-directed CVD approach for GFs.

1.4.2 Direct Self-Assembly Of Graphene Oxide

The most effective method for designing 3D graphene networks is the self-assembly of GO sheets [41]. In fact, due to GO electrostatic repulsion from the functional groups on GO sheets and van der Waals attraction from the basal planes of GO sheets, in GO suspension, individual GO sheets are well distributed [42]. When the equilibrium between these forces is lost, the gelation of a GO suspension begins which resulting in the interconnection of the GO sheets to form a hydrogel, which produces 3D porous architecture after freeze drying.

During the hydrogel graphene formation, the various supramolecular interaction like van der Waals forces, π - π stacking interactions, electrostatic interactions, hydrogen bonding, and dipole interaction of graphene sheets. Obviously, based on the smaller interlayer spacing of the GO (6.94 Å) comparing to the hydrogel (3.76 Å), the existence of π - π stacking interactions of graphene sheets are investigated [42]. This was triggered by recovering the GO sheets after gelation from π -conjugation. If the dispersion surpassed a certain concentration, chemically converted graphene was discovered to be self-gelated without any extra gelators. Repulsive forces were launched by the hydrophilic, oxygen-containing groups on the surface of the GO [43]. H-bond interaction between functional groups and Hydrophobic interaction between basal planes, together with these forces, led to the self-assembly of GO solution.

The critical concentration of the gel is also a significant parameter in the gelation of GO suspensions. GO concentration was 25 mg mL⁻¹ during the dispersion of GO by sonication

is reported by Qin et al. [33]. Although, even when the concentration of GO was 0.065–0.135 mg mL⁻¹ hydrogel will be fabricated – but the mechanical strength of the aerogel is weak. Another study, ammonia was used as a reducing agent in 180 °C for 12 hours. Low density and high mechanical strength are therefore difficult to accomplish at the same time. In this condition, the most common methods for forming hydrogels are self-assembly by means of hydrothermal and chemical reductions [44].

Using the self-assembly strategy, Wu et al [34], are prepared graphene oxide aerogel followed by hydrogen reduction of graphene oxide aerogel to create GA. This graphene aerogel had a large pore size and high surface area. Some various physical treatments such as hydrothermal treatment, direct freeze-drying, controlled centrifugation/filtration, electrochemical deposition was followed by gelation of a GO suspension which takes place by self-assembly of GO sheets. The surface tension inside the gel resists the fluid flow that could interrupt the bonds. There are several methods to initiate GO suspension gelation, such as introducing cross-linkers, altering the pH value of the distributed GO solution, and using chemical reactions [45].

1.4.3 Hydrothermal Reduction Induced Self Assembly

Xu et al. [46], originally developed a hydrothermal one-step technique to make hydrogel graphene. Qin et al [33], reported that hydrogel graphene was able to assist 100 g of weight with little deformation and the GO concentration was smaller (2 mg mL⁻¹) than (30 mg mL⁻¹) for direct gelation. It was thermally stable, electrically conductive, mechanically strong, highly specific capacity. They added ascorbic acid as a reducing agent to the GO solution, then put in a steel autoclave. Afterwards they heated it in 120 °C for 6 hours. They used ascorbic acid as a reducing agent in 120 °C for 6 hours. The mechanical strength of the standard hydrogels is lower than the strong graphene skeleton. Most significantly, the concentration of GO is another factor that influences the morphology and features of 3D graphene. Inspiringly, with increasing hydrothermal reaction time, the degree of GO decreases which has been improved with electrical conductivity, compressive elastic modulus, improved storage modules. Though, the complete graphene aerogel pore quantity

and BET surface area and were decreased after drying as reported by Nguyen et al. Thus, 3D graphene could be used as an optimal framework for creating hierarchical macro-and mesoporous structures by incorporating other functional visitors [47].

CHAPTER 2

MATERIALS & METHODS

2.1 Materials

Potassium permanganate (KMnO_4), sulfuric acid (H_2SO_4), Graphite flakes, phosphoric acid (H_3PO_4), hydrochloric acid (HCl), hydrogen peroxide (H_2O_2), Iron (III) chloride (FeCl_3), ammonia, ascorbic acid, hydroiodic acid (HI).

2.1.1 Graphene Oxide Synthesis with Chemical Exfoliation Technique

Firstly, the synthesis of graphene oxide by modified Hummer's method starts with the mechanically mixture of KMnO_4 with natural graphite flakes. As the sulfuric acid in this mentioned concentration is safer in terms of the concentration, in this new method nitric acid (HNO_3) is substituted by $\text{H}_3\text{PO}_4 / \text{H}_2\text{SO}_4$ acid solution mixture. The mixture of KMnO_4 and graphite flakes with 6:1 mass ratio were added to the one equivalent mass of graphite powder

was put into a glass flask placed in oil bath respectively. It is important to notice that the premixing of the potassium permanganate (KMnO_4) and graphite in the case of the oxidation process [48]. Then, with respect to graphite mass, 9:1 and 1:1 mass ratio of H_2SO_4 and H_3PO_4 , were added to the solid mixture. To prevent a sudden temperature increase, acids should be poured slowly [49]. The mixture solution was followed in an ice bath and then refluxed. The reaction has proceeded for 24 hours in the reflux [50]. After completion of the reaction, the reaction mixture was combined with hydrogen peroxide (H_2O_2), and ice and 20:1 (v:v) ice- H_2O_2 mixture for further neutralization. Washing the solution is the last step in the graphene oxide synthesis after the oxidation process was carried out by centrifugation. To reach to the pH around 3.5, the solution was washed several times with Ethanol-Water. Washed GO was collected by filtration on filters and dried in an oven for 24 hours at 60°C [49-51]. Figure 2.1 represented the stages of material processing in different steps (a to f).

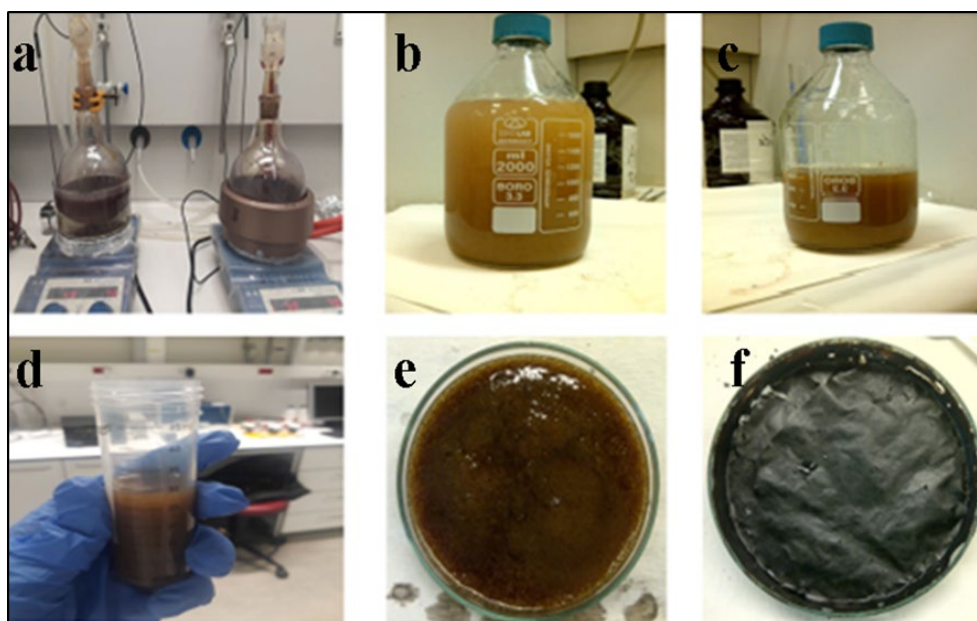


Figure 2. 1 (a) GO synthesis setup, (b) GO suspension before washing, (c) GO suspension after precipitation, (d) Washing process with special centrifuge tube, (e) Collection of the sample, (f) Dried final GO product.

2.2 Fabrication of Graphene Networks

In this study, two techniques were employed: (i) CVD method and the (ii) self-assembly of GO through hydrothermal reduction. There are different techniques of synthesis for 3D graphene including direct synthesis of 3D-Graphene (Template-assisted chemical vapor deposition growth), assembly of Graphene Oxide sheets (Self-assembly of GO through electrochemical reduction, self-assembly of GO through a hydrothermal reduction) and template-assisted assembly [52, 53].

2.2.1 Template-Assisted Chemical Vapor Deposition Growth (CVD)

This method called CVD to grow 3D graphene which is needed to use metal substrates of pre-fabricated 3D such as Ni foam. The Ni foam, in this case, acts as both a template and a catalyst. Then nickel foam was subjected to (CH_4) at 1000°C at constant rates.

First, nickel foams were cut into pieces of $10 \times 10 \text{ mm}^2$ and then placed in a quartz tube. The nickel foams were heated to 1000°C in a horizontal tube furnace under Ar (250 s.c.c.m.) and H_2 (100 s.c.c.m.) and CH_4 (50 s.c.c.m.) annealed for 20 min to clean their surfaces and eliminate a thin surface oxide layer which was followed by adding a small amount of CH_4 into the reaction tube. After 5, 10, 20 min of reaction mixture flow, the samples were cooled to room temperature under Ar and H_2 .

Then the graphene-nickel foam was put into the mixture of HCl (1M) and FeCl_3 (1M) for 24 hours to completely dissolve the nickel to obtain GF [54]. When the nickel was etched away, the GF should be in DI water for 24 hours. In the last step, the GF was dried in the oven. Figure 2.2 showed the steps in different steps.

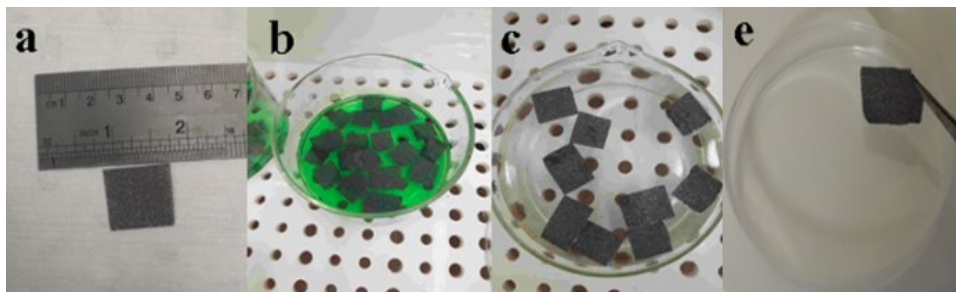


Figure 2. 2 (a) Ni foam, (b) Ni-Graphene foam before etching in FeCl_3/HCL solution, (c) Graphene foam after etching in DI water, (d) Drying Ni foam in 55 C, (e) Graphene foam

2.2.2 Graphene Aerogel (GA) Synthesis

In this work, graphene hydrogel is fabricated via a one-step hydrothermal process in a bottle glasses at 95°C . Since this method generally involves moderate temperature and pressure, graphene sheets self-assemble into 3D graphene occurs by using reduction agents such as hydroiodic acid, hydroquinone, ammonia, Na_2S , ascorbic acid, NaBH_4 . By assembling GO sheets and metal oxide nanoparticles, we prepared a graphene-based aerogel. Graphene aerogel synthesis by simultaneously assembling and reduction GO with ascorbic acid, ammonia, and Hydroiodic acid (HI) as a reduction agent with high electrical conductivity and mechanical characteristics is stated. As one of the most common amine chemicals, Ammonia solution can be used as a GO reducer and stabilizer at the same time. Consequently, ascorbic acid and ammonia solutions are anticipated to cause self-assembly of graphene sheets to form 3D graphene structures under appropriate circumstances by reduction GO.

A new class of ultra-lightweight, extremely compressive 3D Graphene aerogels is being produced with high electrical conductivity. More importantly, the attitude we have reached is highly viable for industry, and low cost and, the temperature (95°C), lower than the GO reduction temperature that reported in the literatures [55-57], aided by freeze-drying procedures to reduce GO with ammonia solution effectively. Furthermore, it can be concluded that the graphene aerogel had extremely reproducible compressibility, high electrical conductivity and surface area.

GO suspensions at different concentrations with different types of reducing agents were prepared. Reducing agents used were Ammonia, HI, Ascorbic Acid and the GO concentrations included in 2, 4, 5, 10, 20, 30 mg.mL⁻¹. For graphene aerogel preparation, 200 μL of reducing agents (ammonia, HI, and ascorbic acid) with a mass percentage of 25% were added gradually into 50 mL of a GO solution. Each sample after adding a reducing agent was sonicated for 10 min in sonication bath to achieve a homogeneous dispersion.

Then, the mixed solution was transferred into a bottle glass and heated at 95 °C for 24 hours. The reactor was cooled down naturally at room temperature. The obtained hydrogel was subsequently taken out, washed until a pH value of 7 was reached, and freeze-dried to prepare GA. Also, the different temperature was considered as a parameter to explore the formation of 3D graphene structure. After reaction, temperature reaches over 95 °C, the black monolith can be observed. The process of preparation of the graphene hydrogel is used in characterization based on the following conditions: The solution of 4 mg mL⁻¹ GO with the 200 μL ammonia solution were mixed and then heated to 95°C and kept for 24 h. By the freeze-drying method graphene hydrogel graphene aerogel was produced.

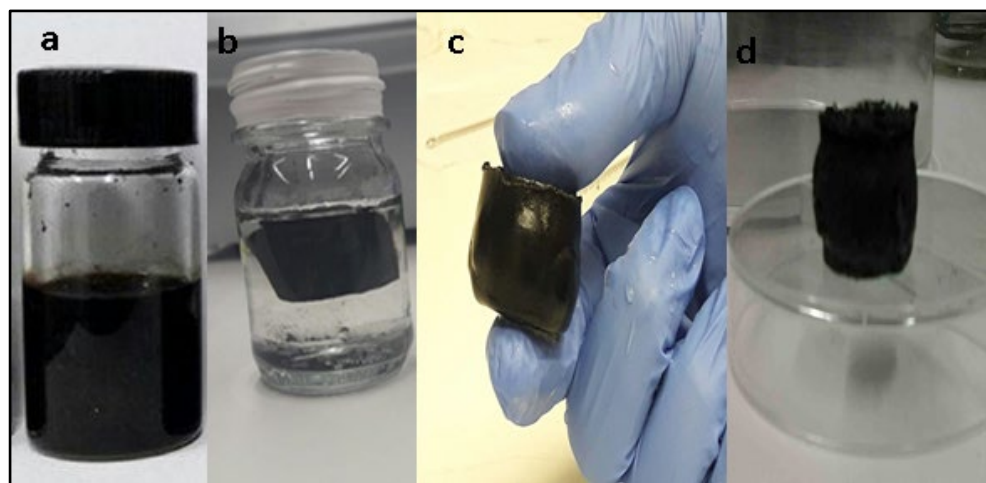


Figure 2. 3 Synthesis of graphene aerogels: (a) GO aqueous dispersion, (b) graphene hydrogel, (c) washed graphene aerogels and (d) dried graphene aerogels.

2.3 Self-Assembled Fe₂O₃/Graphene Aerogel

2.3.1 Preparation of Fe₂O₃-Graphene Composites

FeCl₃.6H₂O (135 mg) and ascorbic acid (400 mg) were dissolved in 20 mL deionized water. Due to the high mechanical strength and moderate electrical conductivity compared to other materials, ascorbic acid was chosen as a reducing agent.

After that, 80 mg graphene sheets were also dispersed in 20 mL deionized water to prepare 4 mg mL⁻¹ GO suspension, and the GO suspension was ultrasonicated for 1 h. Then the GO solution was added slowly to the previous FeCl₃ precursor solution. The mixture suspension was sealed in a Teflon lined stainless steel autoclave. The mixture hydrothermally treated at 95 °C and kept at this temperature for 6 h [61-63].

After cooling to room temperature, the precipitate Fe₂O₃-graphene hydrogel was collected after copious washing by deionized water. Next, the as-prepared hydrogel was freeze-dried for one day.

2.4 Electrochemical Characterization Studies

Graphene foam prepared with CVD method was used as working electrodes to investigate the Li-ion storage characteristics graphene foam. The battery was made of 3D-graphene foam as the anode, lithium chip as reference electrode, Li-ion battery separator and lithium Hexafluorophosphate solution in ethylene carbonate and dimethyl carbonate, 1.0 M LiPF₆ in EC / DMC=50/50 (v / v) as electrolyte.

The cell with graphene foam anode was tested for comparison of electrochemical behavior by cyclic voltammetry (CV). CV was recorded at a scan rate of 0.1 mV s⁻¹ in a potential range of 0–3 V [64]. Galvanostatic charge-discharge measurements were conducted within cut-off potentials 0.1–4 V at the current density of 0.4 mA cm⁻² at ambient temperature on a battery testing system.

CHAPTER 3

RESULTS & DISSCUSSION

3.1 Structural and Electrochemical Properties of Graphene Aerogel (Part I)

3.1.1 Thermal Characterization

Thermogravimetric analysis was performed at temperature range from 30 ° C to 1100 ° C to evaluate the thermal stability of the graphene foam [65]. Figure 3.1 shows GF analytical thermogravimetric profiles. The initial temperature of the pristine GF sample is about 290 ° C. A small weight loss of graphene foam observed before 250 ° C. After 350 ° C, the first significant weight loss was occur due to the oxidation of carbon. No significant weight loss at temperatures above 550 ° C was noted. The same associated weight loss typically can be observed around 690 °C in other studies.

The initial weight of Fe₂O₃/GA was 28.01 mg and after finishing the process at 1099.4 °C the residual mass was 7.69 mg. According to the weight loss, it is estimated that the mass percentage of Fe₂O₃ particles in the composite is about 27.5%.

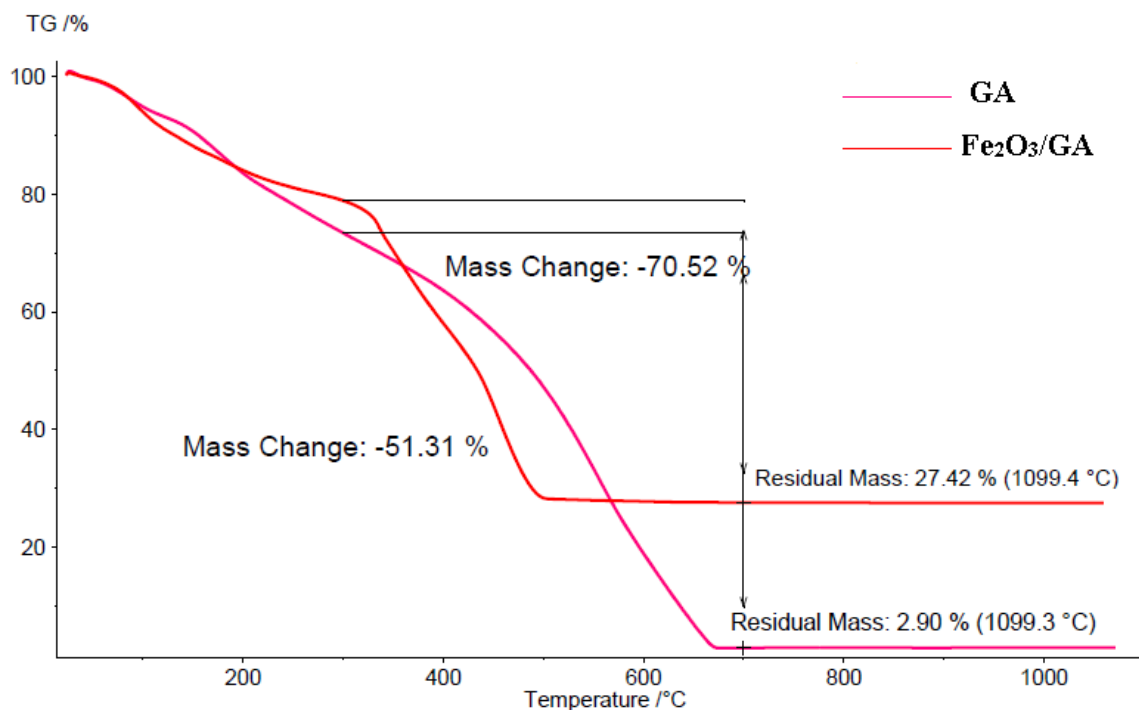


Figure 3. 1 Thermogravimetric analysis of 3D graphene foam/ Fe₂O₃ prepared with hydrothermal reduction method.

The iron oxide (II) in gamma and alpha polymorphs can be decomposed to form iron (III) oxide-hydroxide. The magnitude of this thermal decomposition is directly associate to the particle size. The difference between two graphs represents the impurity in chemical phases and the effect of iron oxide (II) on decomposition of GO.

3.1.2 XRD and Raman Characterization

Raman spectroscopy measurements were carried out using a 532 nm laser source in a Renishaw InVia Reflex Raman microscopy system at Sabanci University. Figure 3.2 shows

the ammonia, HI and ascorbic acid peaks of GO and GAs. For all measured samples, two distinctive bands were noted at 1347 cm⁻¹ and 1588 cm⁻¹ corresponding to the D and G bands.

These bands represent the defects and disorders in the graphite-like materials. The intensity ratio of D and G bands (I_D / I_G) of the GAs reduced by ammonia (1.01), Ascorbic acid (1.05) and HI (1.08) is larger than that of the GO (0.98), indicating that the disordered graphene sheets and defective structures have been improved for the obtained GAs.

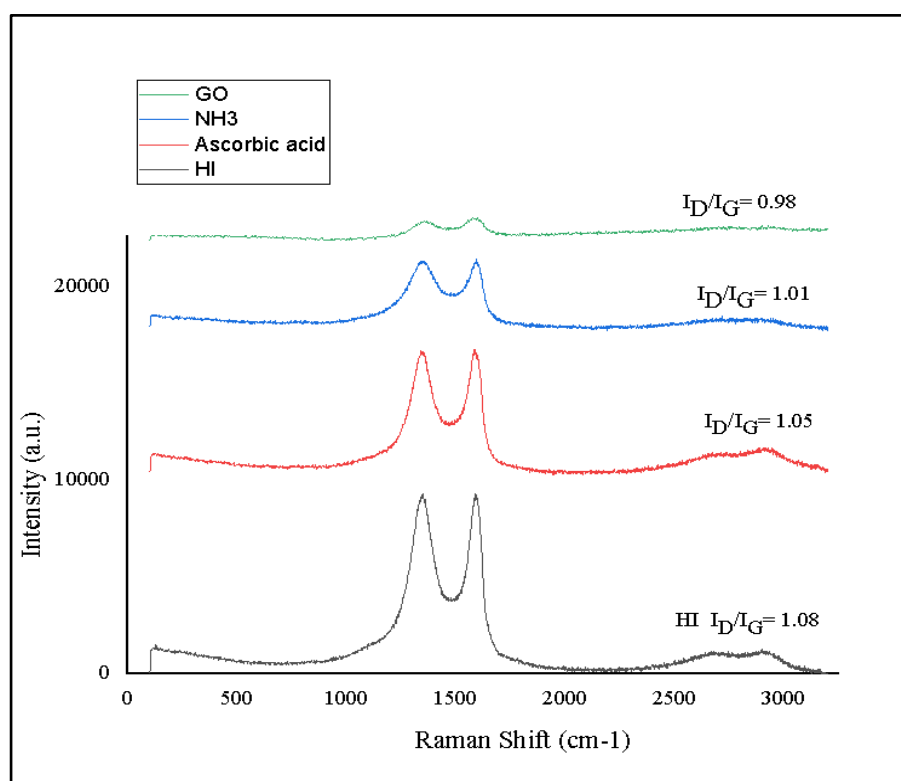


Figure 3. 2 Raman spectra of GO and GAs reduced by ammonia, ascorbic acid, and HI at 95°C.

Figure 3.3 shows the Raman spectra of the graphene and iron oxide graphene aerogel samples. As it is shown, in the graphene aerogel sample, two peaks at 1347 and 1588 cm⁻¹ were found, showing the existence of the D band and G band. IG band was supposed to be the E2 g mode for sp² graphitic carbon, and D band was associated with carbon indicating

structural defects. Consequently, the ID / IG intensity ratio may represent the degree of disorder in the crystal structure.

The D and G band intensity ratio (ID / IG) is a helpful measure for evaluating the carbon crystal structures that are ordered or disordered. Raman's Fe₂O₃/GA sample analysis showed a slight increase in D and G graphene ID / IG bands in Fe₂O₃/GA (1.09) compared to GAs (1.01, 1.05, 1.08). Furthermore, the 580 cm⁻¹ Raman band shows the existence of nanoparticles from Fe₂O₃. The Raman band is assigned to A₁g mode at 214 cm⁻¹ and the E_g mode band at 271 cm⁻¹. Fe₂O₃/GA aerogels provides proof that Fe is attached to the reduced GO sheets.

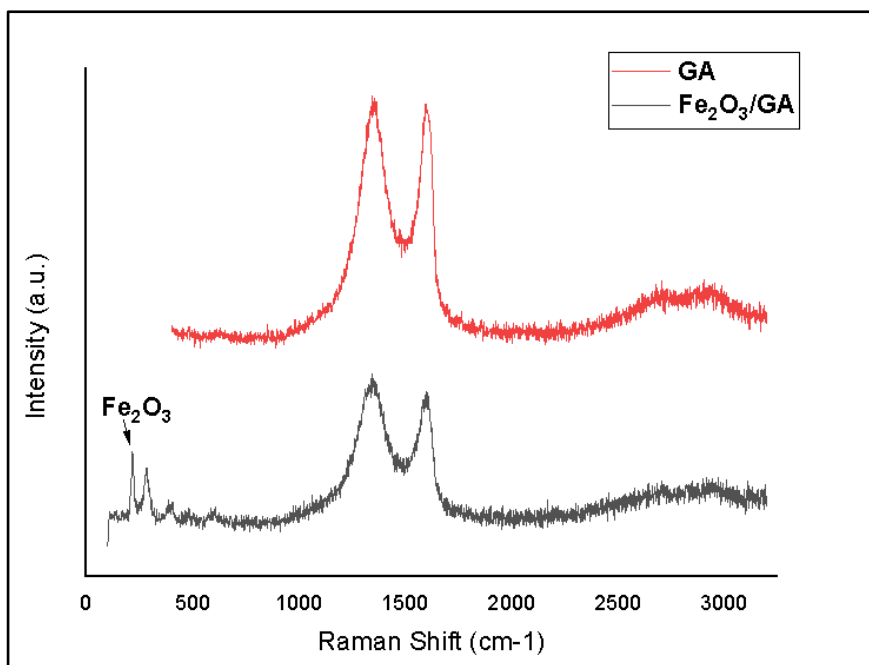


Figure 3. 3 Raman spectra of GA and Fe₂O₃/GA prepared with ascorbic as a reducing agent in 95 °C.

X-ray Diffraction (XRD) were performed to reveal crystal structure of samples, between 2 θ values of 2–90° with Bruker AXS D8 Advance diffractometer (Cu-K line $\lambda = 1.5406 \text{ \AA}$). As it is shown in Figure 3.3, the related XRD pattern, the graphene aerogel's main XRD peak

backs up to 25.1° after hydrothermal reaction and then drying. This indicates the recovery of graphitic crystal structure.

The X-ray diffract-gram of graphene aerogel with $\text{Fe}_2\text{O}_3/\text{GA}$ by similar processing shows that: (I) the graphene sheets peaks are going to disappear which represent that the graphene sheets are homogenously dispersed in Fe_2O_3 matrix and the sheets overlap did not happen at 25.1° (2 θ) and (II) the x-ray spectrum of the hybrid aerogel are same as Fe_2O_3 Powder [66-68]. As it can be seen in figure 3.4, the formation of $\alpha\text{-Fe}_2\text{O}_3/\text{GA}$ is verified by peaks of 24.1° , 33.5° , 35.8° and 41° , that indexed to (012), (104), (110) and (113) crystal planes of $\alpha\text{-Fe}_2\text{O}_3$ respectively. The x-ray spectra proves the crystalline form of $\alpha\text{-Fe}_2\text{O}_3$ particles that are anchored on FLG sheets. The 25.1° peak can be allocated to (002) plane of the graphene sheets illustrate that the presence of graphene sheets cannot effect on iron oxide crystallization [69].

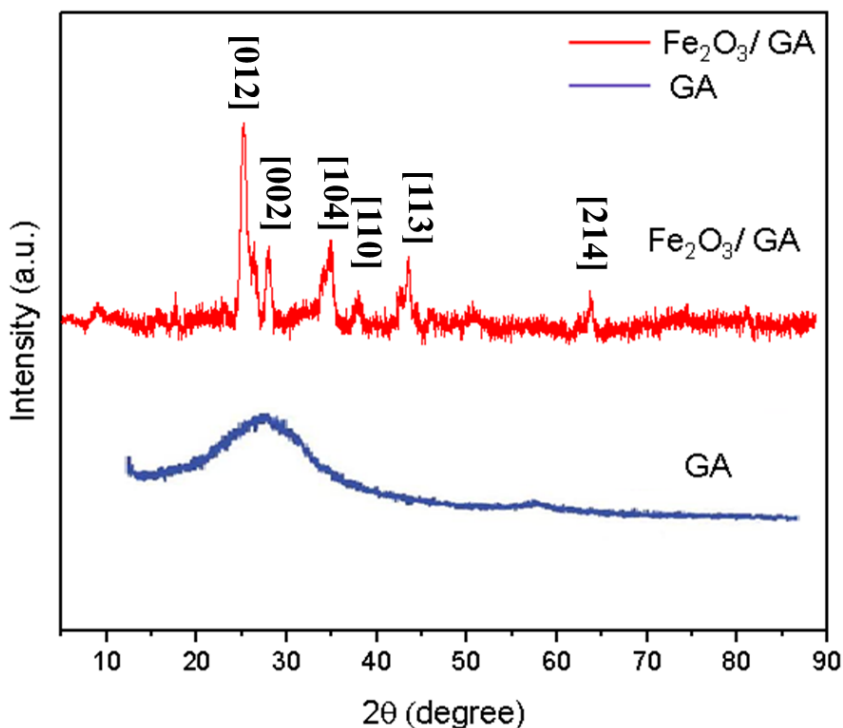


Figure 3. 4 XRD patterns of GA and $\text{Fe}_2\text{O}_3/\text{GA}$ prepared with ascorbic as a reducing agent in 95°C .

3.1.3 SEM Characterization

Scanning electron microscopy (SEM) images were provided on a field emission scanning electron micro analyzer (Zeiss LEO Supra 35 VP) at an acceleration voltage 5 kV in order to monitor the orientation and packing degree of GO fibers.

By means of electron microscopy, it was shown that pore sizes of the graphene aerogel (40 μm) reduced by ammonia with 4 mg / mL concentration are more uniform and the pore walls consisting of graphene sheets are thinner (Figure 3.5a) than that of the GAs reduced by ascorbic acid (Figure 3.5b). The pore walls consisting of graphene sheets are markedly dense and the surface is occupied by some small graphene fragments. In a typical hydrothermal process, the hydrophobic graphene sheets are gradually restored from the GO solution and assemble into a hydrogel.

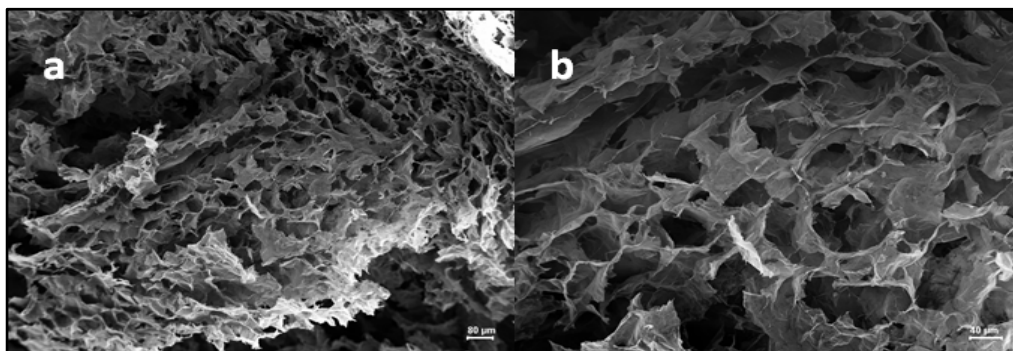


Figure 3. 5 SEM images of the GAs prepared by (a) ammonia, (b) ascorbic acid at 95°C.

Compared to the graphene aerogel which is prepared from 4 mg mL⁻¹ GO aqueous dispersion with ascorbic acid as a reducing agent (Figure 3.6a), the GAs prepared from other concentrations of GO aqueous dispersion also show abundant pore structure. It's worth noting that the pore size gradually reduced with the increased GO concentration from 4 mg mL⁻¹ to 30 mg mL⁻¹ (Figure 3.6b & 3.6c), and the pore structure of graphene aerogel were prepared from 30 mg mL⁻¹ GO was more closely and disorderly (Figure 3.6d).

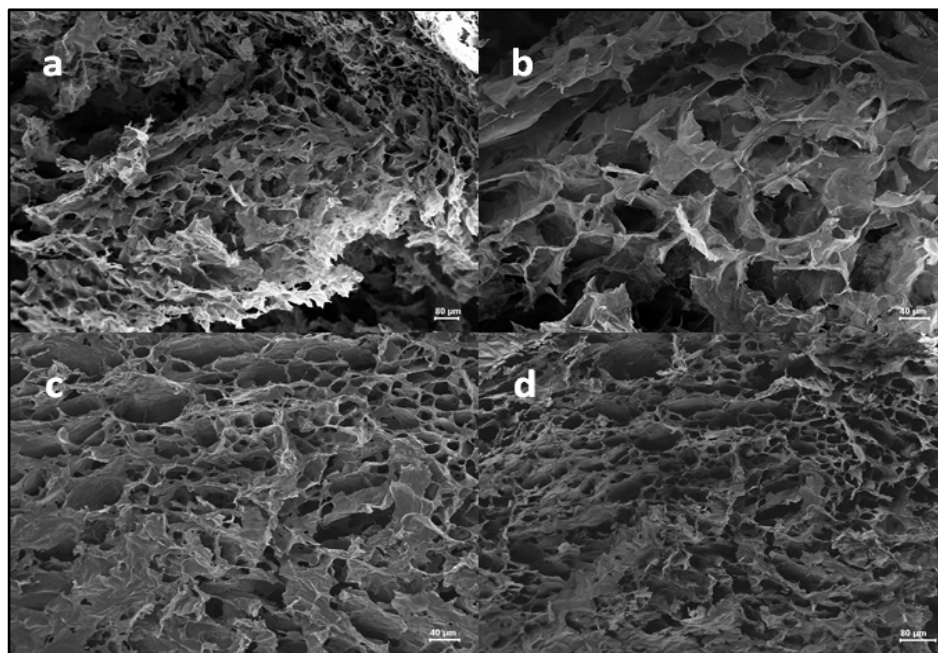


Figure 3. 6 SEM images of graphene aerogel prepared using GO dispersions at different concentration of (a) 4 (b) 5, (c) 10 (d) 30 mg mL⁻¹.

Figure 3.7 shows SEM images of Fe₂O₃/Graphene aerogel. A large amount of pristine Fe₂O₃ nanoparticles is shown. It can be shown that Fe₂O₃ nanoparticles (300 – 500 nm) and nanosheets are spread on nanosheets of graphene. Fig. 16d demonstrates obviously that Fe₂O₃ nano particles are joined with graphene nanosheets and therefore graphene nanosheets are divided by Fe₂O₃ nano particles as well [69].

Obviously, the Fe₂O₃ particles were anchored evenly on both sides of the graphene sheets, and the morphology and microstructure of the as-prepared Fe₂O₃ graphene aerogel was also elucidated by the Fe₂O₃/GAs SEM cross-section. It is worth noting that within the sheets of graphene some Fe₂O₃ particles can be summarized, which can effectively help Fe₂O₃ particles and electrolyte prevent aggregation and avoid direct contact between them. The results also revealed graphene aerogel as a rather thin, interconnected 3D microstructure with multiple micrometer uniformly distributed pores, suggesting an efficient assembly between particles and graphene sheets during hydrothermal treatment.

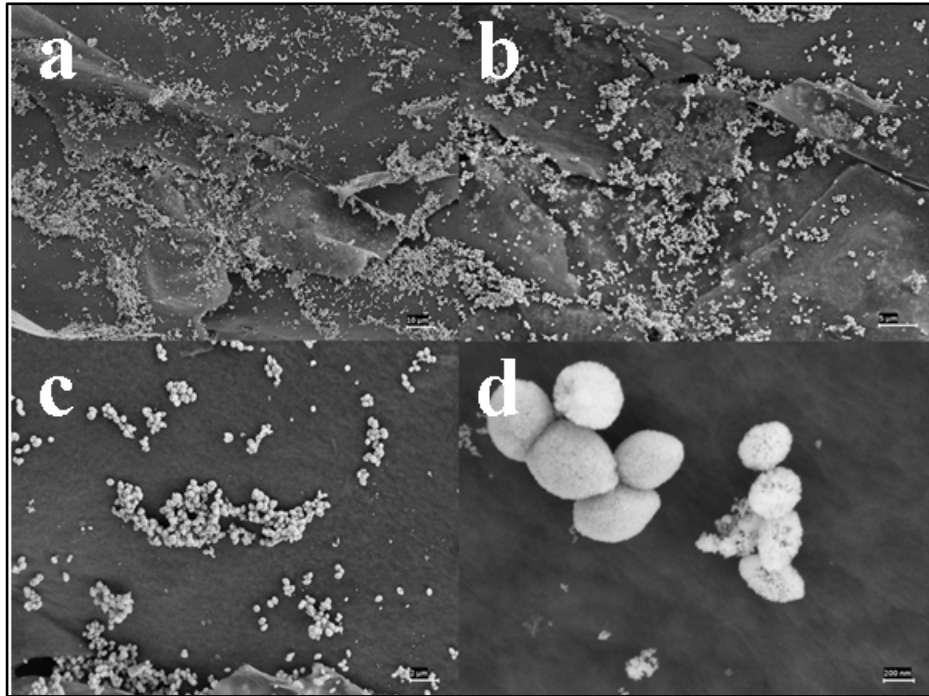


Figure 3. 7 Typical SEM images of Fe₂O₃/GAs revealing the 3D microporous structure and uniform distribution of Fe₂O₃ particles.

3.1.4 Electrical Conductivity Analysis

The electrical conductivity of graphene aerogels was measured by the four-probe method with metal electrodes attached to the ends of samples. The current was passed through metal electrodes attached to either end of the graphene aerogel, and the voltage drop was measured over the aerogel [70].

The measurement of bulk conductivity is like that of sheet conductivity except that a conduction in cm⁻³ is reported using the compact graphene foam as a disc with the thickness, t:

$$\rho = \frac{\pi}{\ln(2)} t \left(\frac{V}{I} \right) = 4.523t \left(\frac{V}{I} \right) \quad (3-1)$$

Where t is 0.7 mm.

The bulk electrical conductivity of 3D graphene networks were less than 1 S/m. The electrical conductivity of graphene aerogels increased after hydrothermal process. The effect of ammonia, ascorbic acid, and HI as reducing agents on the electrical conductivity of the graphene aerogels is considered. It has been found that the electrical conductivity of the hydrogel prepared by using ascorbic acid has higher value compared to others [70].

The GAs' electrical conductivity was evaluated using a four-probe technique and calculated from the linear voltage-current curve. The GAs reduced by HI has the highest electrical conductivity (12.1S/m), but the ammonia and AA-reduced GAs had relatively lower electrical conductivities of 9.4 and 7.5 S/m, respectively (Figure 3.8). The variations in GAs' electrical conductivity reduced by different reduction agents can be explained by the variations in morphology. Due to the more tightly packed nanostructure that enhances electron transport, the graphene aerogel with a reduced surface area has greater electrical conductivity [40, 42].

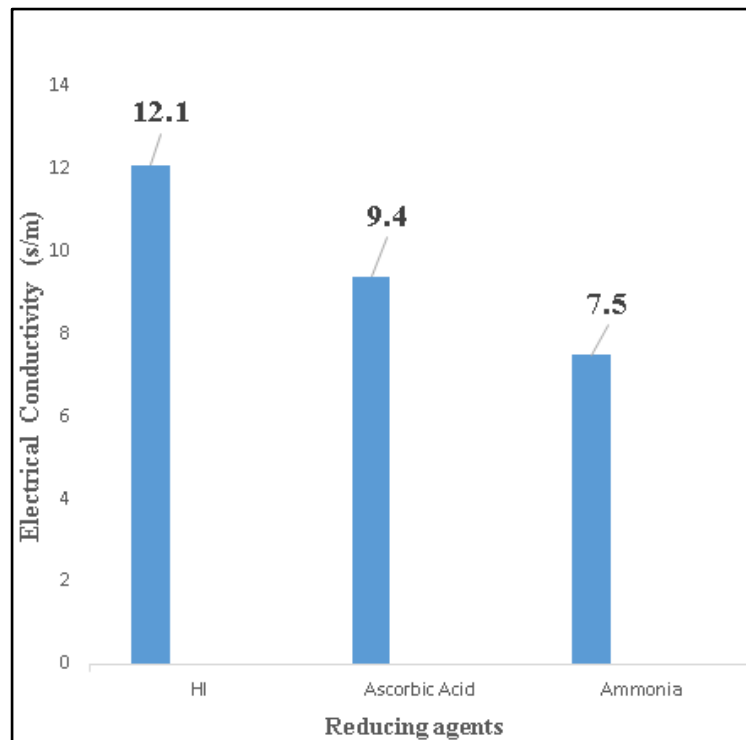


Figure 3. 8 GAs' electrical conductivity with different reducing agents.

3.1.5 Mechanical Characterization

Firstly, the mechanical strength of graphene aerogel prepared with ascorbic acid as reducing agent and concentrated GO (4 mg mL^{-1}) is evaluated with the 102 g loading weight to investigate its compressive strength, compressibility, and recoverability. After putting the sample under the load of 102g, which was over 1000 times more than its own weight (compared in Figure 3.9 a, b), it can recover to its initial form after the static load after release (see Figure 3.9 c, d, e). This specification is exclusively associated to the sample that is prepared with ascorbic acid as reducing agent. The results indicated that the graphene aerogel has an excellent compressive mechanical strength.

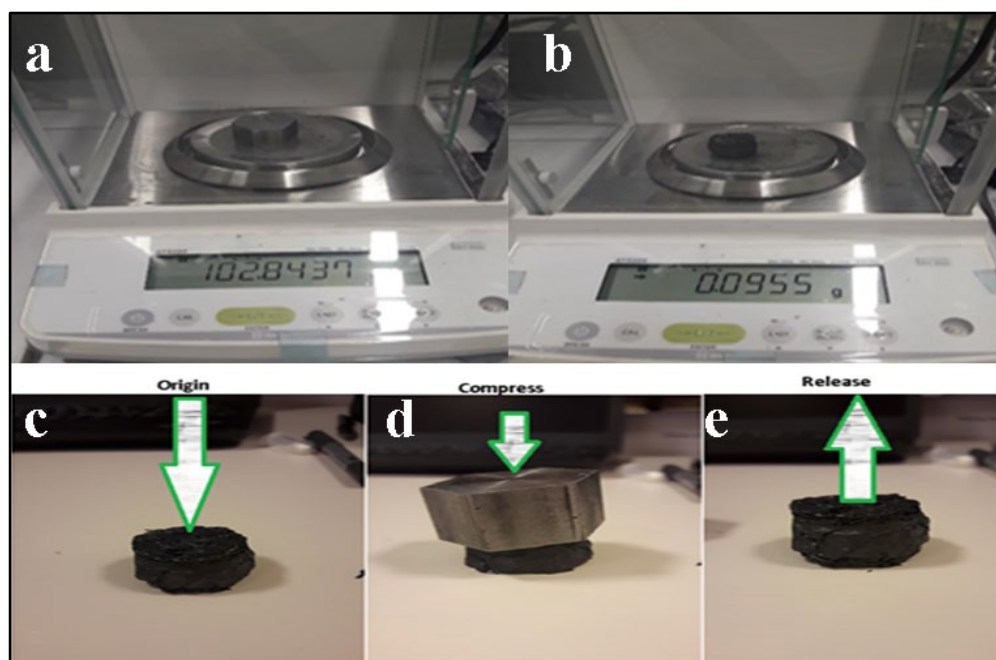


Figure 3. 9 Optical images showing high compressibility of graphene aerogel.

3.1.6 Effect of Different Reducing Agent on Graphene Aerogel Properties

In this study, we systematically investigate the effects of various reducing agents including ammonia, HI, and ascorbic acid. Based on our previous reaction conditions, we first set the temperature to $95 \text{ }^{\circ}\text{C}$ with a 24-hour reaction period to examine the role of the reduction

agent. In terms of mechanical properties, the foam prepared with ascorbic acid had better compressibility but worth electrical properties. The foam made by ammonia had better electrical conductivity than the previous one, but the mechanical properties is worse. Then, we examine HI as a reducing agent, the electrical properties, in this case, was the best, but in terms of mechanical properties, it was worse case among other reducing agents.

3.1.7 Effect of synthesis time on Graphene Aerogel Properties

As can be seen in Figure 3.10, the synthesis time has a significant effect on the shape of the graphene hydrogel. Chemical reduction occurs when the mixture of GO and reducing agent's solution was heated to 95 °C [58], and after 4 h the suspension got dark and homogeneous which follows by the formation of a cylindrical aggregate after 8 h. As the reaction continuous, the π - π conjugated and the hydrophobic structures of the reduced GO sheets increases which results in a compact 3D structure which can be formed because of the steric hindrance effect [59]. Furthermore, the graphene hydrogel could not be obtained when the initial concentration of GO was less than 2.0 mg mL⁻¹.

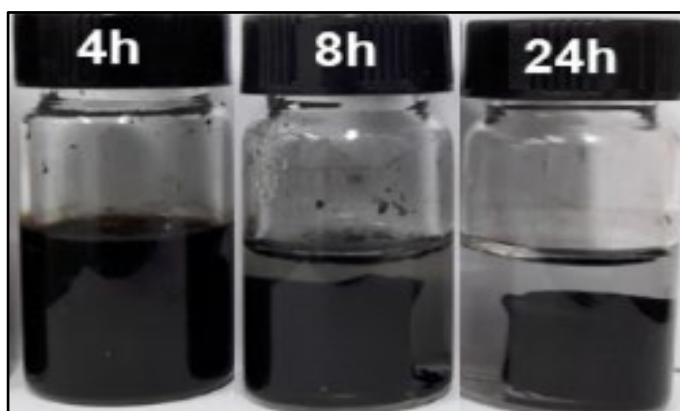


Figure 3. 10 Appearance of the prepared graphene hydrogel after the GO (4 mg mL⁻¹) reacted with ammonia solution at 95°C for different reaction times.

3.1.8 Effect of Reducing Agent Dosage on Graphene Aerogel Properties

After adding the 200 μL of ammonia solution to the GO, the graphene aerogel begins to form. Since GO cannot be properly reduced at low ammonia levels, partly decreased graphene is not powerful enough to create a 3D structure [60]. The reduction of some graphene sheets occur in several steps which the first one is coming from partially reduced GO, and then hydrophobicity of the graphene sheets which causes aggregation [61]. Figure 3.11 illustrate the appearance of the graphene aerogel with different ammonia amounts.

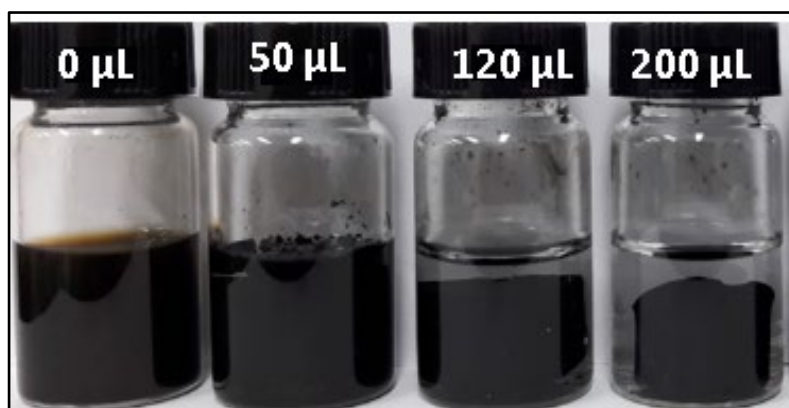


Figure 3. 11 Appearance of the prepared graphene hydrogel after the GO (4 mg mL^{-1}) reacted with different dosage of ammonia at $95 \text{ }^\circ\text{C}$.

GO suspensions at different concentrations with different types of reducing agents were prepared. Reducing agents that is used contains Ammonia, HI, Ascorbic Acid and the GO concentrations: 2, 4, 5, 10, 20, 30 mg mL^{-1} . For graphene aerogel preparation, 200 mL of reducing agents (ammonia, HI, and ascorbic acid) with a mass percentage of 25% were added gradually into 50 mL of a GO solution.

3.2 Structural and Electrochemical Properties of Graphene Foam Prepared with CVD Method (Part 2)

3.2.1 XRD and Raman Characterization

Figure 3.12 shows the diffractogram of the deposited multilayered graphene foam growth on the Ni-foam and etched afterward comparing to pure nickel foam. As it is shown, a low Bragg angle crystalline peak ($2\theta = 26.6^\circ$) emerged that is corresponding to the typical multilayered graphene peak (002). It can be inferred that the formation of multilayered graphene on the Ni-foam surface was successful.

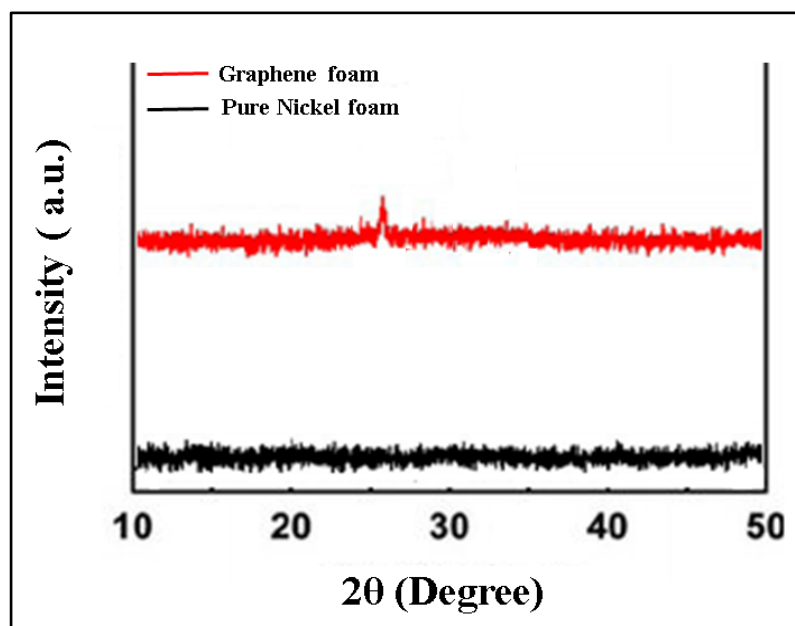


Figure 3. 10 XRD patterns of graphene foam and pure nickel foam.

Figure 3.13 illustrates typical Raman spectra of graphene foam prepared in two different growth time (10 and 20 min). Both spectrum indicated the D, G, and 2D bands. The D-band Raman scattering peak, centered at 1346 cm^{-1} , shows the existence of structural defects in graphene, including point defects, dislocation-like defects, bending of bilayers or multilayers, replacement impurities and carbon atoms, etc. The second peak at around 1570 cm^{-1} is the

G band contributing to the doubly degenerate phonon mode of carbon sp^2 bonds, and this band certifies the presence of graphene. The third peak that is located at approximately 2700 cm^{-1} is the known 2D band induced by the second zone-boundary phonon order. The 2D/G ratios for 10- and 20-min growth are 0.4 and 0.53 respectively. I2D/IG is an indication about layer of graphene to calculate them. The quality of graphene is modified by intercalation and will tend to enhancing of I2D/IG. The I2D/IG intensity ratio, G band peak position and the shape of the 2D band evolve with the number of graphene layers.

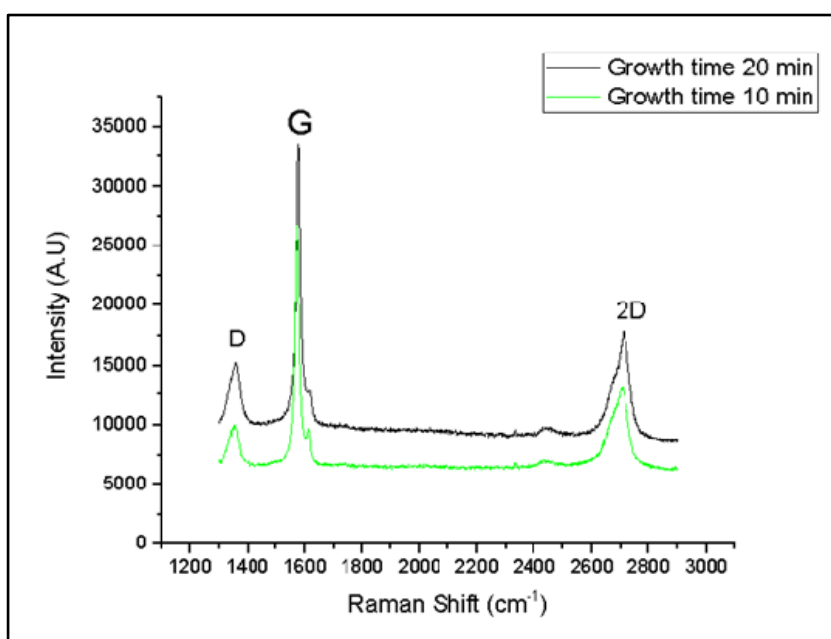


Figure 3. 11 Raman spectra of graphene foam prepared with CVD method in 10 and 20 minutes.

3.2.2 SEM Characterization CVD

The SEM micrographs in figure 3.14a show that the 3D Ni-foam is a porous, soft surface structure. On the surface of the Ni-foam (Figure 3.14b) graphene layers with distinct wrinkles were coated after the CVD process. Because of the structural template effect, the Ni-foam 3D configuration was preserved in all cases. There are a number of wrinkles and ripples

created on the nickel foam that may be due to the distinction between the graphene and nickel thermal expansion coefficients.

As it is shown in figure 3.14c, after etching the nickel, the 3D graphene shaped remained as nickel template's interconnected 3D scaffold structure. This is demonstrating structural integrity and stability. These materials' pore size primarily distributed within the range of $300\mu\text{m}$ that is resembling the nickel foam pore size.

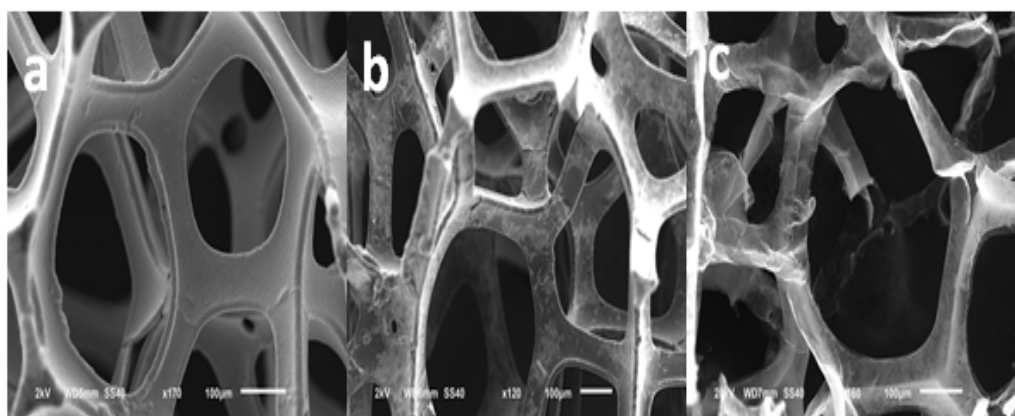


Figure 3. 12 SEM images of (a) bare 3D Ni foam, (b) Nickel-Graphene foam (graphene deposited on the Ni foam), and (c) Graphene foam.

3.2.3 Electrochemical Characterization

Figure 3.15 shows CV curves of the graphene foam prepared with CVD methods, measured at a scan rate of 0.1 mVs^{-1} within a potential range of $0.01\text{--}3\text{ V}$. As it can be seen the graphene foam peak shows the lithiation/delithiation. The initial electrolyte interface layer formation reflected by a peak at 0.8 V , the main reduction peaks at around 0.15 V and 0.02 V , and the oxidation peak at around 0.27 V . Thus, in the prepared anode system, GF was recorded to be electrochemical active against lithium.

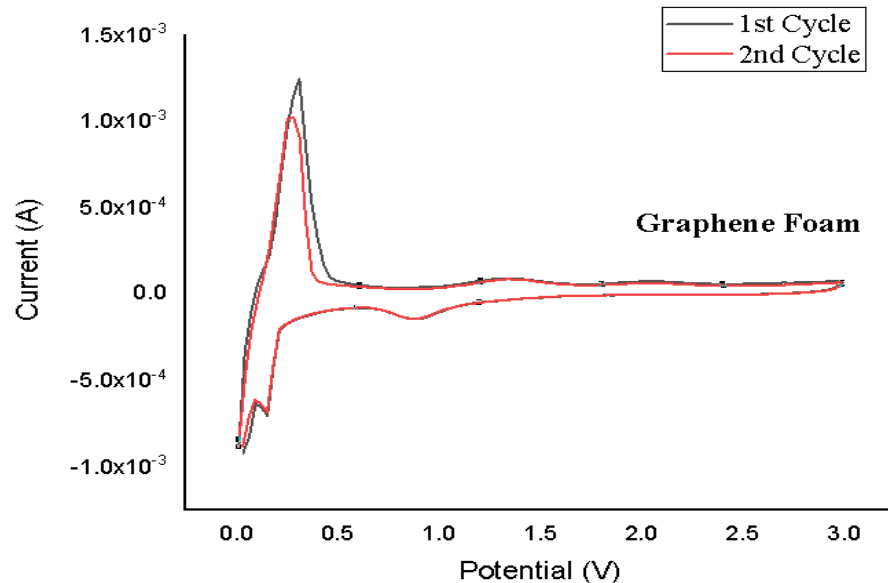


Figure 3. 15 Cyclic voltammetry of graphene foam at a scan rate of 0.1 mV s^{-1} .

Figure 3.16 shows the galvanostatic cycling results of the as-prepared GF sample recorded at a current rate of 0.4 mA cm^{-2} within $0.1\text{--}3 \text{ V}$. It demonstrates the potential profiles with a magnified inset of the potential curves for the 1st, 20th, 50th, and 100th cycles. The lithiation/delithiation plateaus correspond to the obtained CV data and were revealed to be similar for all cycles. In general, lithium ions have the insertion reactions with GF at the potential onset around 0.27 V . The delithiation from GF can be seen to start at around 0.27 V . The GF has a significant contribution to the capacity during the initial 50 cycles. The GF intercalation ability increases upon cycling as well that can be evidenced by extension of the GF delithiation plateau. Thus the overall capacity of the first charge constituted of around 250 mAh/g , where GF contributed. In fact, in the initial cycles, the capacity from GF was around 250 mAh/g , corresponding to that of graphite, and increases up to 280 mAh/g upon a prolonged cycling.

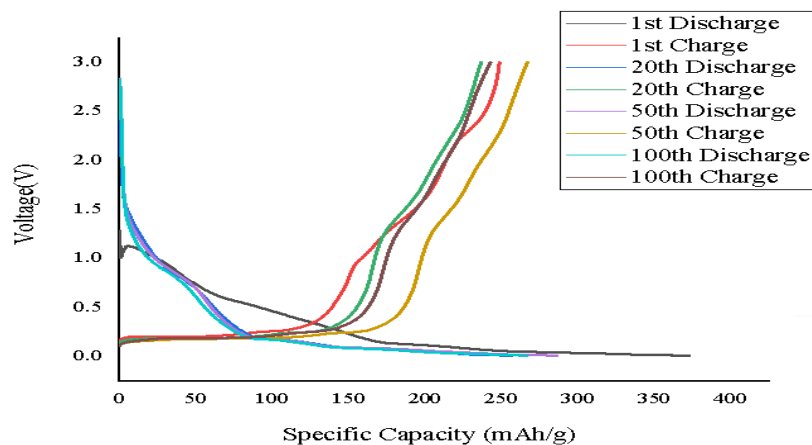


Figure 3. 16 Discharge/charge profiles of graphene foam at current rate of 0.4 mA cm^{-2} between 0.01 and 3 V: the discharge curves in the first, 20th, 50th, 100th.

Figure 3.17 shows the cycling performance of the GF anode system, a reversible capability of up to 280 mA h g^{-1} could still be maintained at the end of 100 charge – discharge cycles. In the first cycle the capacity that was about 370 mA h g^{-1} , after 4 cycles it follows a slight decrease to 260 mA h g^{-1} , but could be maintained at a steady value around 270 mA h g^{-1} till end of 100 charge – discharge cycles.

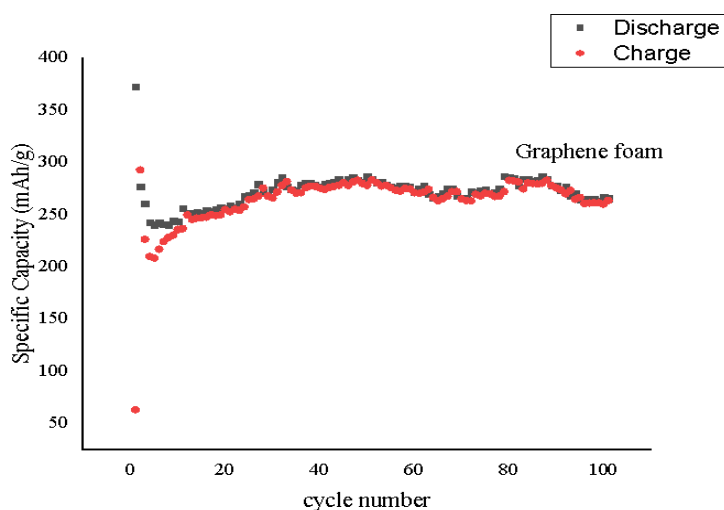


Figure 3. 17 cycling performance of graphene foam at the current density of 185 mA g^{-1} .

CHAPTER 4

CONCLUSION

4.1 Conclusion

In summary, the ultra-light weight 3D Graphene foams were prepared using CVD technique and a chemical reaction by reducing ammonia, ascorbic acid, and HI solutions. The results indicated that the GAs synthesized with a more effective reducing agent showed good electrical conductivity, whereas those with low-efficiency reducing agent had low electrical conductivity. The HI-reduced graphene aerogel shows the worst mechanical strength, and the ammonia-reduced graphene aerogel is very sensitive to the time and temperature of the reaction compared to other reduction agents. Although there was the greatest mechanical strength and excellent electrical conductivity in the graphene aerogel reduced by ascorbic acid. These findings provide insight into the optimization of graphene aerogel nanostructure and characteristics for different applications, including electrode growth, energy storage devices, and Nano-composites.

Considering multiple variables, ascorbic acid is a promising reduction agent for the hydrothermal process, as the graphene aerogel produced does not only have outstanding mechanical characteristics but also reveals a broad hydrothermal preparation window.

On the other side, CVD is an advanced path of synthesis, involving the use of costly equipment, limiting huge manufacturing. The hydrothermal technique is very prominent compared to the CVD method, which provides many benefits such as mild circumstances and adjustable parameters of response to prepare a graphene aerogel with great mechanical strength, low density, super-elasticity and potential for reuse.

5. REFERENCES

1. Rogers JA, Someya T, Huang YG, *Science*, 2010, 327(5973):1603–1607.
2. Nishide H, Oyaizu K, *Science*, 2008, 319(5864):737–738.
3. Tarascon JM, Armand M, *Nature*, 2001, 414(6861):359–367.
4. Kang B, Ceder G, *Nature*, 2009, 458(7235):190–193.
5. Zhang HG, Yu XD, Braun PV, *Nature Nanotechnology*, 2011, 6(5):277–281.
6. Pushparaj VL, *Proceedings of the National Academy of Sciences of the United States of America*, 2007, 104(34):13574–13577.
7. Amatucci GG, Badway F, Du Pasquier A, Zheng T, *Journal of the Electrochemical Society*, 2001, 148:A930–A939.
8. Nam KT, *Science*, 2006, 312(5775):885–888.
9. Liu B, *Nano Lett*, 2012 12(6):3005–3011.
10. Jia XL, *Chemical Communications*, 2011, 47(34):9669–9671.
11. Hu LB, Wu H, La Mantia F, Yang Y, Cui Y, *ACS Nano*, 2010, 4(10):5843–5848.
12. Lima MD, 2011, *Science*, 331(6013):51–55.
13. Gwon H, *Energy & Environmental Science*, 2011, 4:1277–1283.
14. Taberna PL, Mitra S, Poizot P, Simon P, Tarascon JM, *Nature Materials*, 2006, 5(7):567–573.
15. Kang KS, Meng YS, Bréger J, Grey CP, Ceder G, *Science*, 2006, 311(5763):977–980.
16. Aricò AS, Bruce P, Scrosati B, Tarascon JM, van Schalkwijk W, *Nature Materials*, 2005, 4(5):366–377.

17. Lee S, Cho Y, Song H-K, Lee KT, Cho J, *Angewandte Chemie International Edition*, 2012, 124:8878–8882.
18. Feckl JM, Fominykh K, Döblinger M, Fattakhova-Rohlfing D, Bein T, *Angewandte Chemie International Edition*, 2012, 51(30):7459–7463.
19. Chen ZP, *Nature Materials*, 2011, 10(6):424–428.
20. Nelson PA, Owen JR, *Journal of the Electrochemical Society*, 2003, 150: A1313–A1317.
21. Aldon L, *Chemistry of Materials*, 2004, 16:5721–5725.
22. Lee YJ, *Science*, 2009, 324(5930):1051–1055.
23. Luo JY, Xia YY, *Advanced Functional Materials*, 2007, 17:3877–3884.
24. Lee SW, *Nature Nanotechnology*, 2010, 5(7):531–537
25. Shin JY, Samuelis D, Maier J, *Advanced Functional Materials*, 2011, 21:3464–3472.
26. Ergang NS, *Advanced Materials*, 2006, 18:1750–1753.
27. Cheng, H. M. & Li, F. Charge delivery goes the distance. *Science* 356, 581–582 (2017).
28. Ding Y, *Electrochemistry Communications*, 2010, 12:10–13.
29. Zhou XF, Wang F, Zhu YM, Liu ZP, *Journal of Materials Chemistry*, 2011, 21:3353–3358.
30. Tang Y, Huang F, Bi H, Liu Z, Wan D, *Journal of Power Sources*, 2012, 203:130–134.
31. Jung HG, Jang MW, Hassoun J, Sun YK, Scrosati B. *Nature Communications*, 2011, 2:516–520.
32. Hassoun J, Lee KS, Sun YK, Scrosati B, *Journal of the American Chemical Society*, 2011 133(9):3139–3143.
33. Z.GN, *Energy Environ Sci*, 2011, 4:4016–4022.

34. Y. Qin, Q. Peng, Y. Ding, Z. Lin, C. Wang, Y. Li, F. Xu, J. Li, Ye Yuan, X. He, Y. Li, *ACS Nano*, 2015, 99, 8933-8941
35. M. Fernandez-Merino, L. Guardia, J. Paredes, S. Villar-Rodil, P. Solis-Fernandez, A. Martinez-Alonso, and J. Tascon, "Vitamin c is an ideal substitute for hydrazine in the reduction of graphene oxide suspensions," *Journal Of Physical Chemistry C*, vol. 114, no. 14, pp. 6426–6432, 2010.
36. K. K. H. De Silva, H.-H. Huang, and M. Yoshimura, "Progress of reduction of graphene oxide by ascorbic acid," *Applied Surface Science*, vol. 447, pp. 338–346, 2018.
37. D. C. Harris, *Quantitative chemical analysis*. New York: Freeman, 7. ed., 2007.
38. T. Shimada, A. Tamaki, H. Nakai, and T. Homma, "Molecular orbital study on the oxidation mechanism of hydrazine and hydroxylamine as reducing agents for electroless deposition process," *Electrochemistry*, vol. 75, pp. 45–49, 01 2007.
39. Taberna, P. L.; Mitra, S.; Poizot, P.; Simon, P.; Tarascon, J. M, *Nature Materials*, 2006, 5(7) 567– 573
40. L. G. Guex, B. Sacchi, K. F. Peuvot, R. L. Andersson, A. M. Pourrahimi, V. Strom, S. Farris, " and R. T. Olsson, "Experimental review: chemical reduction of graphene oxide (go) to reduced graphene oxide (rgo) by aqueous chemistry," *Nanoscale*, vol. 9, no. 27, pp. 9562–9571, 2017.
41. J. Gao, F. Liu, Y. Liu, N. Ma, Z. Wang, and X. Zhang, "Environment-friendly method to produce graphene that employs vitamin c and amino acid," *Chemistry of Materials*, vol. 22, no. 7, pp. 2213–2218, 2010.
42. Reddy, M. V.; Yu, T.; Sow, C. H.; Shen, Z. X.; Lim, C. T.; Subba Rao, G. V.; Chowdari, B. V. R, *Advanced Functional Materials*, 2007, 17 (15)2792– 2799
43. Larcher, D.; Masquelier, C.; Bonnin, D.; Chabre, Y.; Masson, V.; Leriche, J.-B.; Tarascon, J.-M., *Journal of the Electrochemical Society*, 2003, 150 (1)A133– A139
44. Zhou, G.; Wang, D.-W.; Li, F.; Zhang, L.; Li, N.; Wu, Z.-S.; Wen, L.; Lu, G. Q.; Cheng, H.-M, *Chemistry of Materials*, 2010, 22 (18) 5306– 5313

45. Wu, Y.; Wei, Y.; Wang, J.; Jiang, K.; Fan, S, *Nano Letters*, 2013, 13(2) 818– 823
46. Xu, Y., Sheng K., Li C., Shi G., *ACS Nano*, 2010. 4(7), 4324-4330
47. Kang, E.; Jung, Y. S.; Cavanagh, A. S.; Kim, G.-H.; George, S. M.; Dillon, A. C.; Kim, J. K.; Lee, J, *Advanced Functional Materials*, 2011, 21 (13) 2430– 2438
48. Ban, C.; Wu, Z.; Gillaspie, D. T.; Chen, L.; Yan, Y.; Blackburn, J. L.; Dillon, A. C., *Advanced Materials*, 2010, 22 (20)E145– E149
49. Chan, C. K.; Peng, H.; Liu, G.; McIlwrath, K.; Zhang, X. F.; Huggins, R. A.; Cui, Y, *Nature Nanotechnology*, 2008, 3 (1) 31–35
50. Luo, Y.; Luo, J.; Jiang, J.; Zhou, W.; Yang, H.; Qi, X.; Zhang, H.; Fan, H. J.; Yu, D. Y. W.; Li, C. M.; Yu, T, *Science* , 2012, 5 (4) 6559–6566
51. Luo, J.; Xia, X.; Luo, Y.; Guan, C.; Liu, J.; Qi, X.; Ng, C. F.; Yu, T.; Zhang, H.; Fan, H. J, *Advanced Energy Materials*, 2013, 3 (6) 737– 743
52. Arico, A. S.; Bruce, P.; Scrosati, B.; Tarascon, J.-M.; van Schalkwijk, W, *Nature Materials*, 2005, 4 (5) 366–377
53. Magasinski, A.; Dixon, P.; Hertzberg, B.; Kvit, A.; Ayala, J.; Yushin, G, *Nature Materials*, 2010, 9 (4) 353–358
54. Zhang, H.; Yu, X.; Braun, P. V, *Nature Nanotechnology*, 2011, 6 (5) 277– 281
55. Koo, B.; Xiong, H.; Slater, M. D.; Prakapenka, V. B.; Balasubramanian, M.; Podsiadlo, P.; Johnson, C. S.; Rajh, T.; Shevchenko, E. V, *Nano Letters*, 2012, 12 (5) 2429– 2435
56. Song, Y.; Qin, S.; Zhang, Y.; Gao, W.; Liu, J, *The Journal of Physical Chemistry A*, C 2010, 114 (49)21158– 21164
57. Lei, D.; Zhang, M.; Qu, B.; Chen, L.; Wang, Y.; Zhang, E.; Xu, Z.; Li, Q.; Wang, T. *Nanoscale*, 2012, 4 (11) 3422– 3426
58. Yang, S.; Sun, Y.; Chen, L.; Hernandez, Y.; Feng, X.; Müllen, K, *Scientific Reports*, 2012, 2, 427

59. Wang, B.; Chen, J. S.; Wu, H. B.; Wang, Z.; Lou, X. W, J. Am. Chemical Society, 2011,133 (43) 17146– 17148
60. Liu, J.; Zhou, W.; Lai, L.; Yang, H.; Hua Lim, S.; Zhen, Y.; Yu, T.; Shen, Z.; Lin, J, Nano Energy, 2013, 2 (5) 726– 732
61. Zhu, X.; Zhu, Y.; Murali, S.; Stoller, M. D.; Ruoff, R. S, ACS Nano, 2011, 5 (4) 3333– 3338
62. Li, N.; Chen, Z.; Ren, W.; Li, F.; Cheng, H.-M, Proc. Natl. Proceedings of the National Academy of Sciences of the United States of America, 2012, 109 (43) 17360–17365
63. Chen, Z.; Ren, W.; Gao, L.; Liu, B.; Pei, S.; Cheng, H.-M. T, Nature Materials. 2011, 10 (6) 424– 428
64. Liu, J.; Li, Y.; Fan, H.; Zhu, Z.; Jiang, J.; Ding, R.; Hu, Y.; Huang, X, Chemistry of Materials, 2009, 22 (1) 212– 217
65. Karuturi, S. K.; Luo, J.; Cheng, C.; Liu, L.; Su, L. T.; Tok, A. I. Y.; Fan, H. J. A, Advanced Materials, 2012, 24 (30) 4157– 4162
66. Marichy, C.; Bechelany, M.; Pinna, N, Advanced Materials, 2012, 24 (8) 1017– 1032
67. Luo, J.; Karuturi, S. K.; Liu, L.; Su, L. T.; Tok, A. I. Y.; Fan, H. J, Scientific Reports, 2012, 2, 451
68. Wang, X.; Tabakman, S. M.; Dai, H, J. Am. Chemical Society, 2008, 130 (26) 8152– 8153
69. Jandhyala, S.; Mordi, G.; Lee, B.; Lee, G.; Floresca, C.; Cha, P.-R.; Ahn, J.; Wallace, R. M.;Chabal, Y. J.; Kim, M. J.; Colombo, L.; Cho, K.; Kim, J, ACS Nano, 2012, 6 (3) 2722– 2730
70. Martinson, A. B. F.; DeVries, M. J.; Libera, J. A.; Christensen, S. T.; Hupp, J. T.; Pellin, M. J.;Elam, J. W, The Journal of Chemical Physics, C2011, 115 (10) 4333– 4339